

Semi-Exact Control Functionals From Sard's Method

Leah F. South¹, Toni Karvonen², Chris Nemeth³,
Mark Girolami^{4,2}, Chris. J. Oates^{5,2}

¹Queensland University of Technology, Australia

²The Alan Turing Institute, UK

³Lancaster University, UK

⁴University of Cambridge, UK

⁵Newcastle University, UK

May 25, 2022

Abstract

This paper focuses on the numerical computation of posterior expected quantities of interest, where existing approaches based on ergodic averages are gated by the asymptotic variance of the integrand. To address this challenge, a novel technique is proposed to post-process Markov chain Monte Carlo output, based on Sard's approach to numerical integration and the control functional method. The use of Sard's approach ensures that our control functionals are exact on all polynomials up to a fixed degree in the Bernstein-von-Mises limit, so that the reduced variance estimator approximates the behaviour of a polynomially-exact (e.g. Gaussian) cubature method. The proposed method is shown to combine the robustness of parametric control variates with the flexibility of non-parametric control functionals across a selection of Bayesian inference tasks. All methods used in this paper are available in the R package **ZVCV**.

Keywords: control variate; Stein operator; variance reduction.

1 Introduction

This paper focuses on computing the integral $I(f) = \int f(\mathbf{x})p(\mathbf{x})d\mathbf{x}$ of a functional f of interest with respect to a distribution admitting a Lebesgue density p that is positive and continuously differentiable on \mathbb{R}^d . In particular, we assume that both p and its gradient can be evaluated pointwise up to an intractable normalization constant. The standard approach to computing $I(f)$ in this context is to simulate the first m steps of a p -invariant Markov chain $(\mathbf{x}^{(i)})_{i=1}^{\infty}$, possibly after an initial burn-in period, and to take the average along the sample path as an approximation

to the integral:

$$I(f) \approx I_{\text{MC}}(f) = \frac{1}{m} \sum_{i=1}^m f(\mathbf{x}^{(i)}). \quad (1)$$

See Chapters 6–10 of Robert and Casella (2013) for background. In this paper \mathbb{E} , \mathbb{V} and \mathbb{C} respectively denote expectation, variance and covariance with respect to the law \mathbb{P} of the Markov chain. Under regularity conditions on p that ensure the Markov chain $(\mathbf{x}^{(i)})_{i=1}^{\infty}$ is aperiodic, irreducible and reversible, the convergence of $I_{\text{MC}}(f)$ to $I(f)$ as $m \rightarrow \infty$ is described by a central limit theorem

$$\sqrt{m}(I_{\text{MC}}(f) - I(f)) \rightarrow \mathcal{N}(0, \sigma(f)^2) \quad (2)$$

where convergence occurs in distribution and, if the chain starts in stationarity,

$$\sigma(f)^2 = \mathbb{V}[f(\mathbf{x}^{(1)})] + 2 \sum_{i=2}^{\infty} \mathbb{C}[f(\mathbf{x}^{(1)}), f(\mathbf{x}^{(i)})]$$

is the asymptotic variance of f along the sample path. See Theorem 4.7.7 of Robert and Casella (2013) and more generally Meyn and Tweedie (1993) for theoretical background. Note that for all but the most trivial function f we have $\sigma(f)^2 > 0$ and hence, to achieve an approximation error of $O_P(\epsilon)$, a potentially large number $O(\epsilon^{-2})$ of calls to f and p are required.

One approach to reduce the computational cost is through the control variate method (Ripley, 1987; Hammersley and Handscomb, 1964), which involves finding an approximation f_m to f which can be exactly integrated under p , such that $\sigma(f - f_m)^2 \ll \sigma(f)^2$. Given a choice of f_m , the standard estimator (1) is replaced with

$$I_{\text{CV}}(f) = \frac{1}{m} \sum_{i=1}^m [f(\mathbf{x}^{(i)}) - f_m(\mathbf{x}^{(i)})] + \underbrace{\int f_m(\mathbf{x})p(\mathbf{x})d\mathbf{x}}_{(*)}, \quad (3)$$

where $(*)$ is exactly computed. This last requirement makes it challenging to develop control variates for general use, particularly in Bayesian statistics where often the density p can only be accessed in its un-normalized form. In the Bayesian context, Assaraf and Caffarel (1999); Mira et al. (2013) and Oates et al. (2017) addressed this challenge by using $f_m = c_m + \mathcal{L}g_m$ where $c_m \in \mathbb{R}$, g_m is a user-chosen parametric or non-parametric function and \mathcal{L} is an operator, for example the Langevin Stein operator (Stein, 1972; Gorham and Mackey, 2015), that depends on p through its gradient and satisfies $\int (\mathcal{L}g_m)(\mathbf{x})p(\mathbf{x})d\mathbf{x} = 0$ under regularity conditions (see Lemma 1). Convergence of $I_{\text{CV}}(f)$ to $I(f)$ has been studied under (strong) regularity conditions and, in particular (i) if g_m is chosen parametrically, then in general $\liminf \sigma(f - f_m)^2 > 0$ so that, even if asymptotic variance is reduced, convergence rates are unaffected; (ii) if g_m is chosen in an appropriate non-parametric manner then $\limsup \sigma(f - f_m)^2 = 0$ and a smaller number $O(\epsilon^{-2+\delta})$, $0 < \delta < 2$, of calls to f , p and its gradient are required to achieve an approximation error of $O_P(\epsilon)$ for the integral (see Oates et al., 2019; Mijatović et al., 2018; Belomestny et al., 2017, 2019b,a). In the parametric case $\mathcal{L}g_m$ is called a *control variate* while in the non-parametric case it is called a *control functional*.

Practical parametric approaches to the choice of g_m have been well-studied in the Bayesian context, typically based on polynomial regression models (Assaraf and Caffarel, 1999; Mira et al., 2013; Papamarkou et al., 2014; Oates et al., 2016; Brosse et al., 2019), but neural networks have also been proposed recently (Wan et al., 2019; Si et al., 2020). In particular, existing control variates based on polynomial regression have the attractive property of being *semi-exact*, meaning that there is a well-characterized set of functions $f \in \mathcal{F}$ for which f_m can be shown to exactly equal f after a finite number of samples m have been obtained. For the control variates of Assaraf and Caffarel (1999) and Mira et al. (2013) the set \mathcal{F} contains certain low order polynomials when p is a Gaussian distribution on \mathbb{R}^d . Those authors term their control variates “zero variance”, but we prefer the term “semi-exact” since a general integrand f will not be an element of \mathcal{F} . Regardless of terminology, semi-exactness of the control variate is an appealing property because it implies that the approximation $I_{CV}(f)$ to $I(f)$ is exact on \mathcal{F} . Intuitively, the performance of the control variate method is related to the richness of the set \mathcal{F} on which it is exact. For example, polynomial exactness of cubature rules is used to establish their high order convergence rates using a Taylor expansion argument (e.g. Hildebrand, 1987, Chapter 8).

The development of non-parametric approaches to the choice of g_m has to-date focused on kernel methods (Oates et al., 2017; Barp et al., 2018), piecewise constant approximations (Mijatović et al., 2018) and non-linear approximations based on selecting basis functions from a dictionary (Belomestny et al., 2017; South et al., 2019). Non-parametric approaches can be motivated using the “double descent” phenomena recently exposed in Belkin et al. (2019), where a regression model based on a large number of features which are sufficiently regularized can, in some circumstances, achieve better predictive performance compared to regression models with a smaller number of predictors selected based on a bias-variance trade-off. Theoretical analysis of non-parametric control variates was provided in the papers cited above, but compared to parametric methods, practical implementations of non-parametric methods are less well-developed.

In this paper we propose a semi-exact control functional method. This constitutes the “best of both worlds”, where at small m the semi-exactness property promotes stability and robustness of the estimator $I_{CV}(f)$, while at large m the non-parametric regression component can be used to accelerate the convergence of $I_{CV}(f)$ to $I(f)$. In particular we argue that, in the Bernstein-von-Mises limit, the set \mathcal{F} on which our method is exact is precisely the set of low order polynomials, so that our method can be considered as an approximately polynomially-exact cubature rule developed for the Bayesian context.

Our motivation comes from the approach to numerical integration due to Sard (1949). Many numerical integration methods are based on constructing an approximation f_m to the integrand f that can be exactly integrated. In this case the integral $I(f)$ is approximated using $(*)$ in (3). In Gaussian and related cubatures, the function f_m is chosen in such a way that polynomial exactness is guaranteed (Gautschi, 2004, Section 1.4). On the other hand, in kernel cubature and related approaches, f_m is an element of a reproducing kernel Hilbert space chosen such that an error criterion is minimized (Larkin, 1970). The contribution of Sard was

to combine these two concepts in numerical integration by choosing f_m to enforce exactness on a low-dimensional space \mathcal{F} of functions and use the remaining degrees of freedom to find a minimum-norm interpolant to the integrand.

The remainder of the paper is structured as follows: Section 2.1 recalls Sard’s approach to integration and Section 2.2 how Stein operators can be used to construct a control functional. The proposed semi-exact control functional estimator I_{SECF} is presented in Section 2.3 and its polynomial exactness in the Bernstein-von-Mises limit is discussed in Section 2.4. A closed-form expression for the resulting estimator I_{CV} is provided in Section 2.5. The statistical and computational efficiency of the proposed semi-exact control functional method is compared with that of existing control variates and control functionals using several simulation studies in Section 3. Practical diagnostics for the proposed method are established in Section 4. The paper concludes with a discussion in Section 5.

2 Methods

In this section we provide background details on Sard’s method and Stein operators before describing the semi-exact control functional method.

2.1 Sard’s Method

Many popular methods for numerical integration are based on either (i) enforcing *exactness* of the integral estimator on a finite-dimensional set of functions \mathcal{F} , typically a linear space of polynomials, or on (ii) integration of a *minimum-norm interpolant* selected from an infinite-dimensional set of functions \mathcal{H} . In each case, the result is a cubature method of the form

$$I_{\text{NI}}(f) = \sum_{i=1}^m w_i f(\mathbf{x}^{(i)}) \quad (4)$$

for weights $\{w_i\}_{i=1}^m \subset \mathbb{R}$ and points $\{\mathbf{x}^{(i)}\}_{i=1}^m \subset \mathbb{R}^d$. Classical examples of methods in the former category are the univariate Gaussian quadrature rules (Gautschi, 2004, Section 1.4), which are determined by the unique $\{(w_i, \mathbf{x}^{(i)})\}_{i=1}^m \subset \mathbb{R} \times \mathbb{R}^d$ such that $I_{\text{NI}}(f) = I(f)$ whenever f is a polynomial of order at most $2m - 1$, and Clenshaw–Curtis rules (Clenshaw and Curtis, 1960). Methods of the latter category specify a suitable normed space $(\mathcal{H}, \|\cdot\|_{\mathcal{H}})$ of functions, construct an interpolant $f_m \in \mathcal{H}$ such that

$$f_m \in \arg \min_{h \in \mathcal{H}} \{ \|h\|_{\mathcal{H}} : h(\mathbf{x}^{(i)}) = f(\mathbf{x}^{(i)}) \text{ for } i = 1, \dots, m \} \quad (5)$$

and use the integral of f_m to approximate the true integral. Specific examples include splines (Wahba, 1990) and kernel or Gaussian process based methods (Larkin, 1970; O’Hagan, 1991; Briol et al., 2019).

If the set of points $\{\mathbf{x}^{(i)}\}_{i=1}^m$ is fixed, the cubature method in (4) has m degrees of freedom corresponding to the choice of the weights $\{w_i\}_{i=1}^m$. The approach proposed by Sard (1949) is a hybrid of the two classical approaches just described, calling

for $q \leq m$ of these degrees of freedom to be used to ensure that $I_{\text{NI}}(f)$ is exact for f in a given q -dimensional linear function space \mathcal{F} and, if $q < m$, allocating the remaining $m - q$ degrees of freedom to select a minimal norm interpolant from a large class of functions \mathcal{H} . The approach of Sard is therefore exact for functions in the finite-dimensional set \mathcal{F} and, at the same time, suitable for the integration of functions in the infinite-dimensional set \mathcal{H} . Further background on Sard’s method can be found in Larkin (1974) and Karvonen et al. (2018).

However, it is difficult to implement Sard’s method, or indeed any of the classical approaches just discussed, in the Bayesian context, since

1. the density p can be evaluated pointwise only up to an intractable normalization constant;
2. to construct weights one needs to evaluate the integrals of basis functions of \mathcal{F} and of the interpolant f_m , which can be as difficult as evaluating the original integral.

To circumvent these issues, in this paper we propose to combine Sard’s approach to integration with Stein operators (Stein, 1972; Gorham and Mackey, 2015), thus eliminating the need to access normalization constants and to exactly evaluate integrals. A brief background on Stein operators is provided next.

2.2 Stein Operators

Let \cdot denote the dot product $\mathbf{a} \cdot \mathbf{b} = \mathbf{a}^\top \mathbf{b}$, $\nabla_{\mathbf{x}}$ denote the gradient $\nabla_{\mathbf{x}} = [\partial_{x_1}, \dots, \partial_{x_d}]^\top$ and $\Delta_{\mathbf{x}}$ denote the Laplacian $\Delta_{\mathbf{x}} = \nabla_{\mathbf{x}} \cdot \nabla_{\mathbf{x}}$. Let $\|\mathbf{x}\| = (\mathbf{x} \cdot \mathbf{x})^{1/2}$ denote the Euclidean norm on \mathbb{R}^d . The construction that enables us to realize Sard’s method in the Bayesian context is the Langevin Stein operator \mathcal{L} (Gorham and Mackey, 2015) on \mathbb{R}^d , defined for sufficiently regular g and p as

$$(\mathcal{L}g)(\mathbf{x}) = \Delta_{\mathbf{x}}g(\mathbf{x}) + \nabla_{\mathbf{x}}g(\mathbf{x}) \cdot \nabla_{\mathbf{x}} \log p(\mathbf{x}). \quad (6)$$

We refer to \mathcal{L} as a Stein operator due to the use of equations of the form (6) (up to a simple substitution) in the method of Stein (1972) for assessing convergence in distribution and due to its property of producing functions whose integrals with respect to p are zero under suitable conditions such as those described in Lemma 1.

Lemma 1. *If $g: \mathbb{R}^d \rightarrow \mathbb{R}$ is twice continuously differentiable, $\log p: \mathbb{R}^d \rightarrow \mathbb{R}$ is continuously differentiable and $\|\nabla_{\mathbf{x}}g(\mathbf{x})\| \leq C\|\mathbf{x}\|^{-\delta}p(\mathbf{x})^{-1}$ is satisfied for some $C \in \mathbb{R}$ and $\delta > d - 1$, then*

$$\int (\mathcal{L}g)(\mathbf{x})p(\mathbf{x})d\mathbf{x} = 0,$$

where \mathcal{L} is the Stein operator in (6).

The proof is provided in Appendix A. Although our attention is limited to (6), the choice of Stein operator is not unique and other Stein operators can be derived using the generator method of Barbour (1988) or using Schrödinger Hamiltonians

(Assaraf and Caffarel, 1999). Contrary to the standard requirements for a Stein operator, the operator \mathcal{L} in control functionals does not need to fully characterize convergence and, as a consequence, a broader class of functions g can be considered than in more traditional applications of Stein’s method (Stein, 1972).

It follows that, if the conditions of Lemma 1 are satisfied by $g_m : \mathbb{R}^d \rightarrow \mathbb{R}$, the integral of a function of the form $f_m = c_m + \mathcal{L}g_m$ is simply c_m , the constant. The main challenge in developing control variates, or functionals, based on Stein operators is therefore to find a function g_m such that the asymptotic variance $\sigma(f - f_m)^2$ is small. To explicitly minimize asymptotic variance, Mijatović et al. (2018); Belomestny et al. (2019a) and Brosse et al. (2019) restricted attention to particular Metropolis–Hastings or Langevin samplers for which asymptotic variance can be explicitly characterized. The minimization of empirical variance has also been proposed and studied in the case where samples are independent (Belomestny et al., 2017) and dependent (Belomestny et al., 2019a,b). For an approach that is not tied to a particular Markov kernel, authors such as Assaraf and Caffarel (1999) and Mira et al. (2013) proposed to minimize mean squared error along the sample path, which corresponds to the case of an independent sampling method. In a similar spirit, the constructions in Oates et al. (2017, 2019) and Barp et al. (2018) were based on a minimum-norm interpolant, where the choice of norm is decoupled from the mechanism from where the points are sampled.

In this paper we combine Sard’s approach to integration with a minimum-norm interpolant construction in the spirit of Oates et al. (2017) and related work; this is described next.

2.3 The Proposed Method

In this section we first construct an infinite-dimensional space \mathcal{H} and a finite-dimensional space \mathcal{F} of functions; these will underpin the proposed semi-exact control functional method.

For the infinite-dimensional component, let $k : \mathbb{R}^d \times \mathbb{R}^d \rightarrow \mathbb{R}$ be a positive-definite *kernel*, meaning that (i) k is symmetric, with $k(\mathbf{x}, \mathbf{y}) = k(\mathbf{y}, \mathbf{x})$ for all $\mathbf{x}, \mathbf{y} \in \mathbb{R}^d$, and (ii) the *kernel matrix* $[\mathbf{K}]_{i,j} = k(\mathbf{x}^{(i)}, \mathbf{x}^{(j)})$ is positive-definite for any distinct points $\{\mathbf{x}^{(i)}\}_{i=1}^m \subset \mathbb{R}^d$ and any $m \in \mathbb{N}$. Recall that such a k induces a unique *reproducing kernel Hilbert space* $\mathcal{G}(k)$. This is a Hilbert space that consists of functions $g : \mathbb{R}^d \rightarrow \mathbb{R}$ and is equipped with an inner product $\langle \cdot, \cdot \rangle_{\mathcal{G}(k)}$. The kernel k is such that $k(\cdot, \mathbf{x}) \in \mathcal{G}(k)$ for all $\mathbf{x} \in \mathbb{R}^d$ and it is *reproducing* in the sense that $\langle g, k(\cdot, \mathbf{x}) \rangle_{\mathcal{G}(k)} = g(\mathbf{x})$ for any $g \in \mathcal{G}(k)$ and $\mathbf{x} \in \mathbb{R}^d$. For $\boldsymbol{\alpha} \in \mathbb{N}_0^d$ the multi-index notation $\mathbf{x}^{\boldsymbol{\alpha}} := x_1^{\alpha_1} \cdots x_d^{\alpha_d}$ and $|\boldsymbol{\alpha}| = \alpha_1 + \cdots + \alpha_d$ will be used. If k is twice continuously differentiable in the sense of Steinwart and Christmann (2008, Definition 4.35), meaning that the derivatives

$$\partial_{\mathbf{x}}^{\boldsymbol{\alpha}} \partial_{\mathbf{y}}^{\boldsymbol{\alpha}} k(\mathbf{x}, \mathbf{y}) = \frac{\partial^{2|\boldsymbol{\alpha}|}}{\partial \mathbf{x}^{\boldsymbol{\alpha}} \partial \mathbf{y}^{\boldsymbol{\alpha}}} k(\mathbf{x}, \mathbf{y})$$

exist and are continuous for every multi-index $\boldsymbol{\alpha} \in \mathbb{N}_0^d$ with $|\boldsymbol{\alpha}| \leq 2$, then

$$k_0(\mathbf{x}, \mathbf{y}) = \mathcal{L}_{\mathbf{x}} \mathcal{L}_{\mathbf{y}} k(\mathbf{x}, \mathbf{y}), \tag{7}$$

where $\mathcal{L}_{\mathbf{x}}$ stands for application of the Stein operator defined in (6) with respect to variable \mathbf{x} , is a well-defined and positive-definite kernel (Steinwart and Christmann, 2008, Lemma 4.34). The kernel in (7) can be written as

$$\begin{aligned} k_0(\mathbf{x}, \mathbf{y}) &= \Delta_{\mathbf{x}} \Delta_{\mathbf{y}} k(\mathbf{x}, \mathbf{y}) + \mathbf{u}(\mathbf{x})^\top \nabla_{\mathbf{x}} \Delta_{\mathbf{y}} k(\mathbf{x}, \mathbf{y}) \\ &\quad + \mathbf{u}(\mathbf{y})^\top \nabla_{\mathbf{y}} \Delta_{\mathbf{x}} k(\mathbf{x}, \mathbf{y}) + \mathbf{u}(\mathbf{x})^\top [\nabla_{\mathbf{x}} \nabla_{\mathbf{y}}^\top k(\mathbf{x}, \mathbf{y})] \mathbf{u}(\mathbf{y}), \end{aligned} \quad (8)$$

where $\nabla_{\mathbf{x}} \nabla_{\mathbf{y}}^\top k(\mathbf{x}, \mathbf{y})$ is the $d \times d$ matrix with entries $[\nabla_{\mathbf{x}} \nabla_{\mathbf{y}}^\top k(\mathbf{x}, \mathbf{y})]_{i,j} = \partial_{x_i} \partial_{y_j} k(\mathbf{x}, \mathbf{y})$ and $\mathbf{u}(\mathbf{x}) = \nabla_{\mathbf{x}} \log p(\mathbf{x})$. If k is radial then (8) can be simplified; see Appendix B. Lemma 2 establishes conditions under which the functions $\mathbf{x} \mapsto k_0(\mathbf{x}, \mathbf{y})$, $\mathbf{y} \in \mathbb{R}^d$, and hence elements of the Hilbert space $\mathcal{G}(k_0)$ reproduced by k_0 , have zero integral. Let $\|\mathbf{M}\|_{\text{OP}} = \sup_{\|\mathbf{x}\|=1} \|\mathbf{M}\mathbf{x}\|$ denote the operator norm of a matrix $\mathbf{M} \in \mathbb{R}^{d \times d}$.

Lemma 2. *If $k: \mathbb{R}^d \times \mathbb{R}^d \rightarrow \mathbb{R}$ is twice continuously differentiable in each argument, $\log p: \mathbb{R}^d \rightarrow \mathbb{R}$ is continuously differentiable, $\|\nabla_{\mathbf{x}} \nabla_{\mathbf{y}}^\top k(\mathbf{x}, \mathbf{y})\|_{\text{OP}} \leq C(\mathbf{y}) \|\mathbf{x}\|^{-\delta} p(\mathbf{x})^{-1}$ and $\|\nabla_{\mathbf{x}} \Delta_{\mathbf{y}} k(\mathbf{x}, \mathbf{y})\| \leq C(\mathbf{y}) \|\mathbf{x}\|^{-\delta} p(\mathbf{x})^{-1}$ are satisfied for some $C: \mathbb{R}^d \rightarrow (0, \infty)$, and $\delta > d - 1$, then*

$$\int k_0(\mathbf{x}, \mathbf{y}) p(\mathbf{x}) d\mathbf{x} = 0 \quad (9)$$

for every $\mathbf{y} \in \mathbb{R}^d$, where k_0 is defined in (7).

The proof is provided in Appendix D. The infinite-dimensional space \mathcal{H} used in this work is exactly the reproducing kernel Hilbert space $\mathcal{G}(k_0)$. The basic mathematical properties of k_0 and the Hilbert space it reproduces are contained in Appendix C and these can be used to inform the selection of an appropriate kernel.

For the finite-dimensional component, let Φ be a linear subspace of twice-continuously differentiable functions with dimension $q - 1$, $q \in \mathbb{N}$, and a basis $\{\phi_i\}_{i=1}^{q-1}$. Define then the space obtained by applying the differential operator (6) to Φ as $\mathcal{L}\Phi = \text{span}\{\mathcal{L}\phi_1, \dots, \mathcal{L}\phi_{q-1}\}$. If the pre-conditions of Lemma 1 are satisfied for each basis function $g = \phi_i$ then linearity of the Stein operator implies that $\int (\mathcal{L}\phi) dp = 0$ for every $\phi \in \Phi$. Typically we will select $\Phi = \mathcal{P}^r$ as the polynomial space $\mathcal{P}^r = \text{span}\{\mathbf{x}^\alpha : \alpha \in \mathbb{N}_0^d, 0 < |\alpha| \leq r\}$ for some non-negative integer r . Note that constant functions are excluded from \mathcal{P}^r since they are in the null space of \mathcal{L} ; when required we let $\mathcal{P}_0^r = \text{span}\{1\} \oplus \mathcal{P}^r$ denote the larger space with the constant functions included. The finite-dimensional space \mathcal{F} is then taken to be $\mathcal{F} = \text{span}\{1\} \oplus \mathcal{L}\Phi = \text{span}\{1, \mathcal{L}\phi_1, \dots, \mathcal{L}\phi_{q-1}\}$.

It is now possible to state the proposed method. Following Sard, we approximate the integrand f with a function f_m that interpolates f at the locations $\mathbf{x}^{(i)}$, is exact on the q -dimensional linear space \mathcal{F} , and minimises a particular (semi-)norm subject to the first two constraints. It will occasionally be useful to emphasise the dependence of f_m on f using the notation $f_m(\cdot) = f_m(\cdot; f)$. The proposed interpolant takes the form

$$f_m(\mathbf{x}) = b_1 + \sum_{i=1}^{q-1} b_{i+1} (\mathcal{L}\phi_i)(\mathbf{x}) + \sum_{i=1}^m a_i k_0(\mathbf{x}, \mathbf{x}^{(i)}), \quad (10)$$

where the coefficients $\mathbf{a} = (a_1, \dots, a_m) \in \mathbb{R}^m$ and $\mathbf{b} = (b_1, \dots, b_q) \in \mathbb{R}^q$ are selected such that the following two conditions hold:

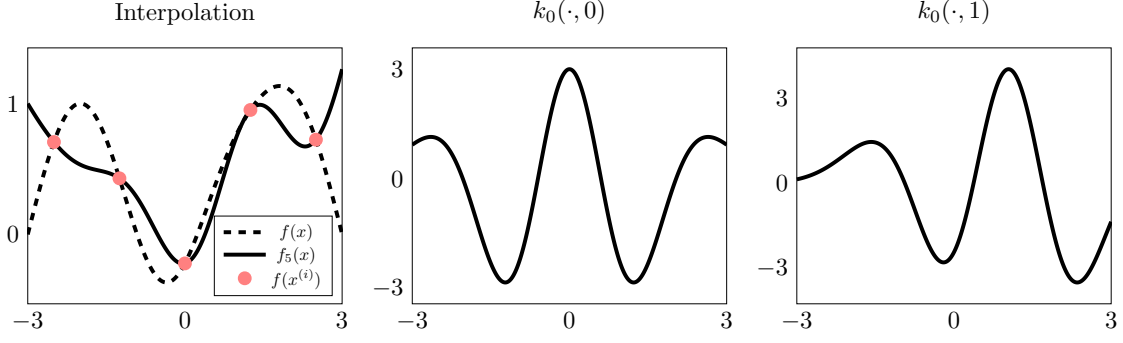


Figure 1: *Left*: The interpolant f_m from (10) at $m = 5$ points to the function $f(x) = \sin(0.5\pi(x-1)) + \exp(-(x-0.5)^2)$ for the Gaussian density $p(x) = \mathcal{N}(x; 0, 1)$. The interpolant uses the Gaussian kernel $k(x, y) = \exp(-(x-y)^2)$ and a polynomial parametric basis with $r = 2$. *Center & right*: Two translates $k_0(\cdot, y)$, $y \in \{0, 1\}$, of the kernel (7).

1. $f_m(\mathbf{x}^{(i)}; f) = f(\mathbf{x}^{(i)})$ for $i = 1, \dots, m$ (interpolation);
2. $f_m(\cdot; f) = f(\cdot)$ whenever $f \in \mathcal{F}$ (semi-exactness).

Since \mathcal{F} is q -dimensional, these requirements correspond to the total of $m + q$ constraints. Under weak conditions, discussed in Section 2.5, the total number of degrees of freedom due to selection of \mathbf{a} and \mathbf{b} is equal to $m + q$ and the above constraints can be satisfied. Furthermore, the corresponding function f_m can be shown to minimise a particular (semi-)norm on a larger space of functions, subject to the interpolation and exactness constraints (to limit scope, we do not discuss this characterisation further but the semi-norm is defined in (16) and the reader can find full details in Wendland, 2004, Theorem 13.1). Figure 1 illustrates one such interpolant. The proposed estimator of the integral is then

$$I_{\text{SECF}}(f) = \int f_m(\mathbf{x})p(\mathbf{x}) \, d\mathbf{x}, \quad (11)$$

a special case of (3) (the interpolation condition causes the first term in (3) to vanish) that we call a *semi-exact control functional*. The following is immediate from (10) and (11):

Corollary 1. *Under the hypotheses of Lemma 1 for each $g = \phi_i$, $i = 1, \dots, q - 1$, and Lemma 2, it holds that, whenever the estimator $I_{\text{SECF}}(f)$ is well-defined, $I_{\text{SECF}}(f) = b_1$, where b_1 is the constant term in (10).*

The earlier work of Assaraf and Caffarel (1999) and Mira et al. (2013) corresponds to $\mathbf{a} = \mathbf{0}$, while setting $\mathbf{b} = \mathbf{0}$ in (10) and ignoring the semi-exactness requirement recovers the unique minimum-norm interpolant in the Hilbert space $\mathcal{H} = \mathcal{G}(k_0)$ where k_0 is reproducing, in the sense of (5). The work of Oates et al. (2017) corresponds to $b_i = 0$ for $i = 2, \dots, q$. It is therefore clear that the proposed approach is a strict generalization of existing work and can be seen as a compromise between semi-exactness and minimum-norm interpolation.

2.4 Polynomial Exactness in the Bernstein-von-Mises Limit

A central motivation for our approach is the prototypical case where p is the density of a posterior distribution $P_{\mathbf{x}|y_1, \dots, y_n}$ for a latent variable \mathbf{x} given independent and identically distributed data $y_1, \dots, y_n \sim P_{y_1, \dots, y_n|\mathbf{x}}$. Under regularity conditions discussed in Section 10.2 of van der Vaart (1998), the Bernstein-von-Mises theorem states that

$$\left\| P_{\mathbf{x}|y_1, \dots, y_n} - \mathcal{N}(\hat{\mathbf{x}}_n, n^{-1}I(\hat{\mathbf{x}}_n)^{-1}) \right\|_{\text{TV}} \rightarrow 0$$

where $\hat{\mathbf{x}}_n$ is a maximum likelihood estimate for \mathbf{x} , $I(\mathbf{x})$ is the Fisher information matrix evaluated at \mathbf{x} , $\|\cdot\|_{\text{TV}}$ is the total variation norm and convergence is in probability as $n \rightarrow \infty$ with respect to the law $P_{y_1, \dots, y_n|\mathbf{x}}$ of the dataset. In this limit, polynomial exactness of the proposed method can be established. Indeed, for a Gaussian density p with mean $\hat{\mathbf{x}}_n \in \mathbb{R}^d$ and precision $nI(\hat{\mathbf{x}}_n)$, if $\phi(\mathbf{x}) = \mathbf{x}^\alpha$ for a multi-index $\alpha \in \mathbb{N}_0^d$, then

$$(\mathcal{L}\phi)(\mathbf{x}) = \sum_{i=1}^d \alpha_i \left[(\alpha_i - 1)x_i^{\alpha_i-2} - \frac{n}{2}P_i(\mathbf{x})x_i^{\alpha_i-1} \right] \prod_{j \neq i} x_j^{\alpha_j},$$

where $P_i(\mathbf{x}) = 2\mathbf{e}_i^\top I(\hat{\mathbf{x}}_n)(\mathbf{x} - \hat{\mathbf{x}}_n)$ and \mathbf{e}_i is the i th coordinate vector in \mathbb{R}^d . This allows us to obtain the following result, whose proof is provided in Appendix E:

Lemma 3. *Consider the Bernstein-von-Mises limit and suppose that the Fisher information matrix $I(\hat{\mathbf{x}}_n)$ is non-singular. Then, for the choice $\Phi = \mathcal{P}^r$, $r \in \mathbb{N}$, the estimator I_{SECF} is exact on $\mathcal{F} = \mathcal{P}_0^r$.*

Thus the proposed estimator is polynomially exact up to order r in the Bernstein-von-Mises limit. At finite n , when the limit has not been reached, the above argument can only be expected to approximately hold.

2.5 Computation for the Proposed Method

The purpose of this section is to discuss when the proposed estimator is well-defined and how it can be computed. Define the $m \times q$ matrix

$$\mathbf{P} = \begin{bmatrix} 1 & \mathcal{L}\phi_1(\mathbf{x}^{(1)}) & \cdots & \mathcal{L}\phi_{q-1}(\mathbf{x}^{(1)}) \\ \vdots & \vdots & \ddots & \vdots \\ 1 & \mathcal{L}\phi_1(\mathbf{x}^{(m)}) & \cdots & \mathcal{L}\phi_{q-1}(\mathbf{x}^{(m)}) \end{bmatrix},$$

which is sometimes called a *Vandermonde* (or *alternant*) matrix corresponding to the linear space \mathcal{F} . Let \mathbf{K}_0 be the $m \times m$ matrix with entries $[\mathbf{K}_0]_{i,j} = k_0(\mathbf{x}^{(i)}, \mathbf{x}^{(j)})$ and let \mathbf{f} be the m -dimensional column vector with entries $[\mathbf{f}]_i = f(\mathbf{x}^{(i)})$.

Lemma 4. *Let the $m \geq q$ points $\mathbf{x}^{(i)}$ be distinct and \mathcal{F} -unisolvent, meaning that the matrix \mathbf{P} has full rank. Let k_0 be a positive-definite kernel for which (9) is satisfied. Then $I_{\text{SECF}}(f)$ is well-defined and the coefficients \mathbf{a} and \mathbf{b} are given by the solution of the linear system*

$$\begin{bmatrix} \mathbf{K}_0 & \mathbf{P} \\ \mathbf{P}^\top & \mathbf{0} \end{bmatrix} \begin{bmatrix} \mathbf{a} \\ \mathbf{b} \end{bmatrix} = \begin{bmatrix} \mathbf{f} \\ \mathbf{0} \end{bmatrix}. \quad (12)$$

In particular,

$$I_{\text{SECF}}(f) = \mathbf{e}_1^\top (\mathbf{P}^\top \mathbf{K}_0^{-1} \mathbf{P})^{-1} \mathbf{P}^\top \mathbf{K}_0^{-1} \mathbf{f}. \quad (13)$$

The proof is provided in Appendix F. Notice that (13) is a linear combination of the values in \mathbf{f} and therefore the proposed estimator is recognized as a cubature method of the form (4) with weights

$$\mathbf{w} = \mathbf{K}_0^{-1} \mathbf{P} (\mathbf{P}^\top \mathbf{K}_0^{-1} \mathbf{P})^{-1} \mathbf{e}_1. \quad (14)$$

The requirement in Lemma 4 for the $\mathbf{x}^{(i)}$ to be distinct precludes, for example, the direct use of Metropolis–Hastings output. However, as emphasized in Oates et al. (2017) for control functionals and studied further in Liu and Lee (2017); Hodgkinson et al. (2020), the consistency of I_{SECF} does *not* require that the Markov chain is p -invariant. It is therefore trivial to, for example, filter out duplicate states from Metropolis–Hastings output.

The solution of linear systems of equations defined by an $m \times m$ matrix \mathbf{K}_0 and a $q \times q$ matrix $\mathbf{P}^\top \mathbf{K}_0^{-1} \mathbf{P}$ entails a computational cost of $O(m^3 + q^3)$. In some situations this cost may yet be smaller than the cost associated with evaluation of f and p , but in general this computational requirement limits the applicability of the method just described. In Appendix G we therefore propose a computationally efficient approximation, I_{ASECF} , to the full method, based on a combination of the Nyström approximation (Williams and Seeger, 2001) and the well-known conjugate gradient method, inspired by the recent work of Rudi et al. (2017). All proposed methods are implemented in the R package ZVCV (South, 2020).

3 Empirical Assessment

A detailed comparison of existing and proposed control variate and control functional techniques was performed. Three examples were considered; Section 3.1 considers a Gaussian target, representing the Bernstein-von-Mises limit; Section 3.2 considers a setting where non-parametric control functional methods perform well; Section 3.3 considers a setting where parametric control variate methods are known to be successful. In each case we determine whether or not the proposed semi-exact control functional method is competitive with the state-of-the-art.

Specifically, we compared the following estimators, which are all instances of I_{CV} in (3) for a particular choice of f_m , which may or may not be an interpolant:

- Standard Monte Carlo integration, (1), based on Markov chain output.
- The control functional estimator recommended in Oates et al. (2017), $I_{\text{CF}}(f) = (\mathbf{1}^\top \mathbf{K}_0^{-1} \mathbf{1})^{-1} \mathbf{1}^\top \mathbf{K}_0^{-1} \mathbf{f}$.
- The “zero variance” polynomial control variate method of Assaraf and Caffarel (1999) and Mira et al. (2013), $I_{\text{ZV}}(f) = \mathbf{e}_1^\top (\mathbf{P}^\top \mathbf{P})^{-1} \mathbf{P}^\top \mathbf{f}$.
- The “auto zero variance” approach of South et al. (2019), which uses 5-fold cross validation to automatically select (a) between the ordinary least squares solution I_{ZV} and an ℓ_1 -penalised alternative (where the penalisation strength

is itself selected using 10-fold cross-validation within the test dataset), and (b) the polynomial order.

- The proposed semi-exact control functional estimator, (13).
- An approximation, I_{ASECF} , of (13) based on the Nyström approximation and the conjugate gradient method, described in Appendix G.

Open-source software for implementing all of the above methods is available in the R package **ZVCV** (South, 2020). The same sets of m samples were used for all estimators, in both the construction of f_m and the evaluation of I_{CV} . For methods where there is a fixed polynomial basis we considered only orders $r = 1$ and $r = 2$, following the recommendation of Mira et al. (2013). For kernel-based methods, duplicate values of \mathbf{x}_i were removed (as discussed in Section 2.5) and Frobenius regularization was employed whenever the condition number of the kernel matrix \mathbf{K}_0 was close to machine precision (Higham, 1988). Several choices of kernel were considered, but for brevity in the main text we focus on the rational quadratic kernel $k(\mathbf{x}, \mathbf{y}; \lambda) = (1 + \lambda^{-2} \|\mathbf{x} - \mathbf{y}\|^2)^{-1}$. This kernel was found to provide the best performance across a range of experiments; a comparison to the Matérn and Gaussian kernels is provided in Appendix H. The parameter λ was selected using 5-fold cross-validation, based again on performance across a spectrum of experiments; a comparison to the median heuristic (Garreau et al., 2017) is presented in Appendix H.

To ensure that our assessment is practically relevant, the estimators were compared on the basis of both statistical and computational efficiency relative to the standard Monte Carlo estimator. Statistical efficiency $\mathcal{E}(I_{\text{CV}})$ and computational efficiency $\mathcal{C}(I_{\text{CV}})$ of an estimator I_{CV} of the integral I are defined as

$$\mathcal{E}(I_{\text{CV}}) = \frac{\mathbb{E}[(I_{\text{MC}} - I)^2]}{\mathbb{E}[(I_{\text{CV}} - I)^2]}, \quad \mathcal{C}(I_{\text{CV}}) = \mathcal{E}(I_{\text{CV}}) \frac{T_{\text{MC}}}{T_{\text{CV}}}$$

where T_{CV} denotes the combined wall time for sampling the $\mathbf{x}^{(i)}$ and computing the estimator I_{CV} . For the results reported below, \mathcal{E} and \mathcal{C} were approximated using averages $\hat{\mathcal{E}}$ and $\hat{\mathcal{C}}$ over 100 realizations of the Markov chain output.

3.1 Gaussian Illustration

Here we consider a Gaussian integral that serves as an analytically tractable caricature of a posterior near to the Bernstein-von-Mises limit. This enables us to assess the effect of the sample size m and dimension d on each estimator, in a setting that is not confounded by the idiosyncrasies of any particular MCMC method. Specifically, we set $p(\mathbf{x}) = (2\pi)^{-d/2} \exp(-\|\mathbf{x}\|^2/2)$ where $\mathbf{x} \in \mathbb{R}^d$. For the parametric component we set $\Phi = \mathcal{P}^r$, so that (from Lemma 3) I_{SECF} is exact on polynomials of order at most r ; this holds also for I_{ZV} . For the integrand $f : \mathbb{R}^d \rightarrow \mathbb{R}$, $d \geq 3$, we took

$$f(\mathbf{x}) = 1 + x_2 + 0.1x_1x_2x_3 + \sin(x_1) \exp[-(x_2x_3)^2] \quad (15)$$

in order that the integral is analytically tractable ($I(f) = 1$) and that no method will be exact.

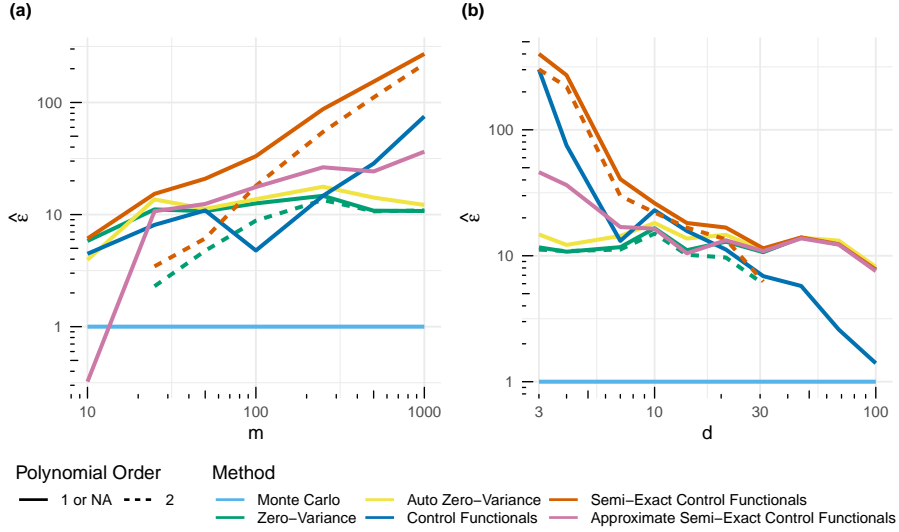


Figure 2: Gaussian example (a) estimated *statistical efficiency* with $d = 4$ and (b) estimated *statistical efficiency* with $m = 1000$ for integrand (15).

Figure 2 displays the statistical efficiency of each estimator for $10 \leq m \leq 1000$ and $3 \leq d \leq 100$. Computational efficiency is not shown since exact sampling from p in this example is trivial. The proposed semi-exact control functional method performs consistently well compared to its competitors for this non-polynomial integrand. Unsurprisingly, the best improvements are for high m and small d , where the proposed method results in a statistical efficiency over 100 times better than the baseline estimator and up to 5 times better than the next best method.

3.2 Capture-Recapture Example

The two remaining examples, here and in Section 3.3, are applications of Bayesian statistics described in South et al. (2019). In each case the aim is to estimate expectations with respect to a posterior distribution $P_{\mathbf{x}|\mathbf{y}}$ of the parameters \mathbf{x} of a statistical model based on \mathbf{y} , an observed dataset. Samples $\mathbf{x}^{(i)}$ were obtained using the Metropolis-adjusted Langevin algorithm (Roberts et al., 1996), which is a Metropolis-Hastings algorithm with proposal $\mathcal{N}(\mathbf{x}^{(i-1)} + h^2 \frac{1}{2} \Sigma \nabla_{\mathbf{x}} \log P_{\mathbf{x}|\mathbf{y}}(\mathbf{x}^{(i-1)} | \mathbf{y}), h^2 \Sigma)$. Step sizes of $h = 0.72$ for the capture-recapture example and $h = 0.3$ for the sonar example (see Section 3.3) were selected and an empirical approximation of the posterior covariance matrix was used as the pre-conditioner $\Sigma \in \mathbb{R}^{d \times d}$. Since the proposed method does not rely on the Markov chain being $P_{\mathbf{x}|\mathbf{y}}$ -invariant we also repeated these experiments using the unadjusted Langevin algorithm (Parisi, 1981; Ermak, 1975), with similar results reported in Appendix I.

In this first example, a Cormack–Jolly–Seber capture-recapture model (Lebreton et al., 1992) is used to model data on the capture and recapture of the bird species *Cinclus Cinclus* (Marzolin, 1988). The integrands of interest are the marginal posterior means $f_i(\mathbf{x}) = x_i$ for $i = 1, \dots, 11$, where $\mathbf{x} = (\phi_1, \dots, \phi_5, p_2, \dots, p_6, \phi_6 p_7)$, ϕ_j is the probability of survival from year j to $j + 1$ and p_j is the probability of

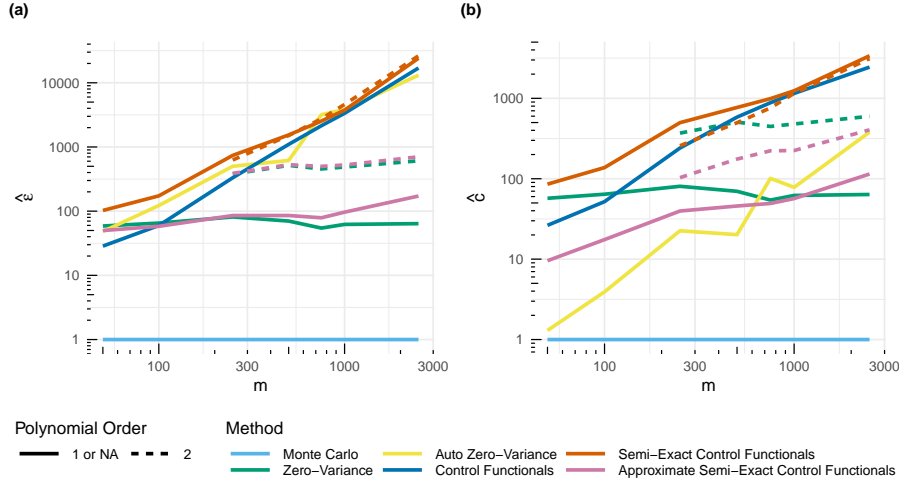


Figure 3: Capture-recapture example (a) estimated *statistical efficiency* and (b) estimated *computational efficiency*. Efficiency here is reported as an average over the 11 expectations of interest.

being captured in year j . The likelihood is

$$\ell(\mathbf{y}|\mathbf{x}) \propto \prod_{i=1}^6 \chi_i^{d_i} \prod_{k=i+1}^7 \left[\phi_i p_k \prod_{m=i+1}^{k-1} \phi_m (1 - p_m) \right]^{y_{ik}},$$

where $d_i = D_i - \sum_{k=i+1}^7 y_{ik}$, $\chi_i = 1 - \sum_{k=i+1}^7 \phi_i p_k \prod_{m=i+1}^{k-1} \phi_m (1 - p_m)$ and the data \mathbf{y} consists of D_i , the number of birds released in year i , and y_{ik} , the number of animals caught in year k out of the number released in year i , for $i = 1, \dots, 6$ and $k = 2, \dots, 7$. Following South et al. (2019), parameters are transformed to the real line using $\tilde{x}_i = \log(x_i/(1 - x_i))$ and the adjusted prior density for \tilde{x}_j is $\exp(\tilde{x}_j)/(1 + \exp(\tilde{x}_j))^2$, for $j = 1, \dots, 11$.

South et al. (2019) found that non-parametric methods outperform standard parametric methods for this 11-dimensional example. The estimator I_{SECF} combines elements of both approaches, so there is interest in determining how the method performs. It is clear from Figure 3 that all variance reduction approaches are helpful in improving upon the vanilla Monte Carlo estimator in this example. The best improvement in terms of statistical and computational efficiency is offered by I_{SECF} , which also has similar performance to I_{CF} .

3.3 Sonar Example

Our final application is a 61-dimensional logistic regression example using data from Gorman and Sejnowski (1988) and Dheeru and Karra Taniskidou (2017). To use standard regression notation, the parameters are denoted $\boldsymbol{\beta} \in \mathbb{R}^{61}$, the matrix of covariates in the logistic regression model is denoted $\mathbf{X} \in \mathbb{R}^{208 \times 61}$ where the first column is all 1's to fit an intercept and the response is denoted $\mathbf{y} \in \mathbb{R}^{208}$. In this application, \mathbf{X} contains information related to energy frequencies reflected from either a metal cylinder ($y = 1$) or a rock ($y = 0$). The log likelihood for this model

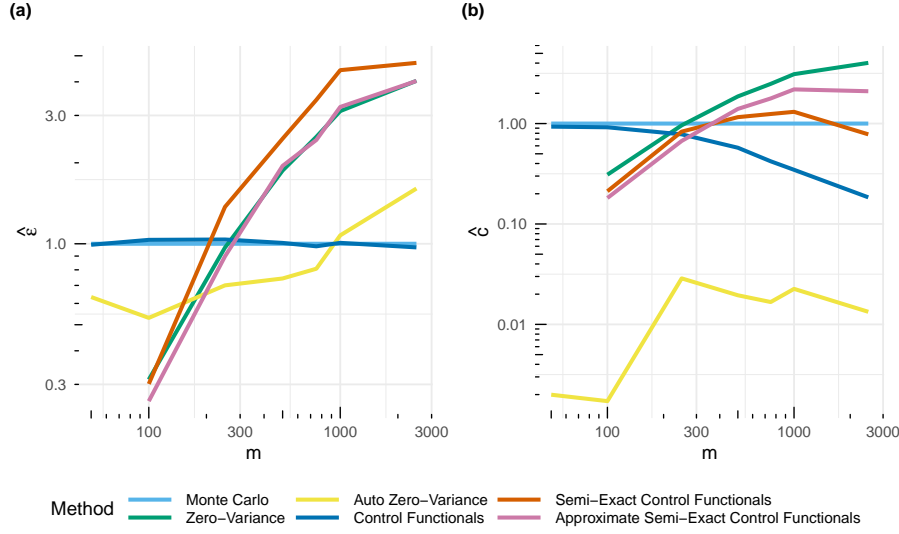


Figure 4: Sonar example (a) estimated *statistical efficiency* and (b) estimated *computational efficiency*.

is

$$\log \ell(\mathbf{y}, \mathbf{X} | \boldsymbol{\beta}) = \sum_{i=1}^{208} (y_i \mathbf{X}_{i,\cdot} \boldsymbol{\beta} - \log(1 + \exp(\mathbf{X}_{i,\cdot} \boldsymbol{\beta}))) .$$

We use a $\mathcal{N}(0, 5^2)$ prior for the predictors (after standardising to have standard deviation of 0.5) and $\mathcal{N}(0, 20^2)$ prior for the intercept, following South et al. (2019); Chopin and Ridgway (2017), but we focus on estimating the more challenging integrand $f(\boldsymbol{\beta}) = (1 + \exp(-\tilde{\mathbf{X}}\boldsymbol{\beta}))^{-1}$, which can be interpreted as the probability that observed covariates $\tilde{\mathbf{X}}$ emanate from a metal cylinder. The gold standard of $I \approx 0.4971$ was obtained from a 10 million iteration Metropolis-Hastings (Hastings, 1970) run with multivariate normal random walk proposal.

Figure 4 illustrates the statistical and computational efficiency of estimators for various m in this example. It is interesting to note that I_{SECF} and I_{ASECF} offer similar statistical efficiency to I_{ZV} , especially given the poor relative performance of I_{CF} . Since it is inexpensive to obtain the m samples using the Metropolis-adjusted Langevin algorithm in this example, I_{ZV} and I_{ASECF} are the only approaches which offer improvements in computational efficiency over the baseline estimator for the majority of m values considered, and even in these instances the improvements are marginal.

4 Theoretical Properties and Convergence Assessment

In this section we provide a convergence result and discuss diagnostics that can be used to monitor the performance of the proposed method. To this end, we introduce

the semi-norm

$$|f|_{k_0, \mathcal{F}} = \inf_{\substack{f=h+g \\ h \in \mathcal{F}, g \in \mathcal{G}(k_0)}} \|g\|_{\mathcal{G}(k_0)}, \quad (16)$$

which is well-defined when the infimum is taken over a non-empty set, otherwise we define $|f|_{k_0, \mathcal{F}} = \infty$.

4.1 Finite Sample Error and a Practical Diagnostic

The following proposition provides a finite sample error bound:

Proposition 1. *Let k_0 be a positive-definite kernel for which (9) is satisfied. Then the integration error satisfies the bound*

$$|I(f) - I_{\text{SECF}}(f)| \leq |f|_{k_0, \mathcal{F}} (\mathbf{w}^\top \mathbf{K}_0 \mathbf{w})^{1/2} \quad (17)$$

where the weights \mathbf{w} , defined in (14), satisfy

$$\mathbf{w} = \arg \min_{\mathbf{v} \in \mathbb{R}^m} (\mathbf{v}^\top \mathbf{K}_0 \mathbf{v})^{1/2} \quad \text{s.t.} \quad \sum_{i=1}^m v_i h(\mathbf{x}^{(i)}) = \int h(\mathbf{x}) p(\mathbf{x}) d\mathbf{x} \quad \text{for every } h \in \mathcal{F}.$$

The proof is provided in Appendix J. The first quantity $|f|_{k_0, \mathcal{F}}$ in (17) can be approximated by $|f_m|_{k_0, \mathcal{F}}$ when f_m is a reasonable approximation for f and this can in turn be bounded as $|f_m|_{k_0, \mathcal{F}} \leq (\mathbf{a}^\top \mathbf{K}_0 \mathbf{a})^{1/2}$. The second quantity $(\mathbf{w}^\top \mathbf{K}_0 \mathbf{w})^{1/2}$ in (17) is computable and is recognized as a *kernel Stein discrepancy* between the empirical measure $\sum_{i=1}^m w_i \delta(\mathbf{x}^{(i)})$ and the distribution whose density is p , based on the Stein operator \mathcal{L} (Chwialkowski et al., 2016; Liu et al., 2016). Note that our choice of Stein operator differs to that in Chwialkowski et al. (2016) and Liu et al. (2016). There has been substantial recent research into the use of kernel Stein discrepancies for assessing algorithm performance in the Bayesian computational context (Gorham and Mackey, 2017; Chen et al., 2018, 2019; Singhal et al., 2019; Hodgkinson et al., 2020) and one can also exploit this discrepancy as a diagnostic for the performance of the semi-exact control functional. The diagnostic that we propose to monitor is the product $(\mathbf{w}^\top \mathbf{K}_0 \mathbf{w})^{1/2} (\mathbf{a}^\top \mathbf{K}_0 \mathbf{a})^{1/2}$. This approach to error estimation was also suggested (outside the Bayesian context) in Section 5.1 of Fasshauer (2011).

Empirical results in Figure 5 suggest that this diagnostic provides a conservative approximation of the actual error. Further work is required to establish whether this diagnostic detects convergence and non-convergence in general.

4.2 Consistency of the Estimator

In this section we establish that, even in the biased sampling setting, the proposed estimator is consistent. The proof exploits a recent theoretical contribution in Hodgkinson et al. (2020). Let Π be the matrix that projects orthogonally onto the columns of $[\Psi]_{i,j} := \mathcal{L}\phi_j(\mathbf{x}^{(i)})$ in the inner product $\langle \cdot, \cdot \rangle_{\mathbf{K}_0^{-1}}$, defined as $\langle \mathbf{u}, \mathbf{v} \rangle_{\mathbf{K}_0^{-1}} = \mathbf{u}^\top \mathbf{K}_0^{-1} \mathbf{v}$.

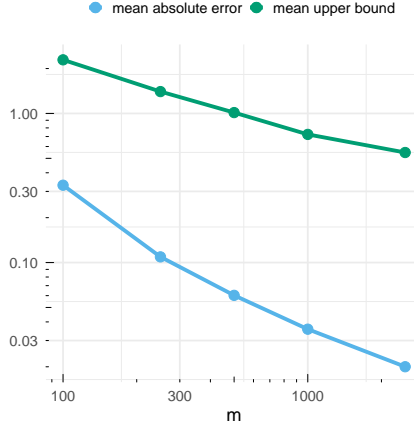


Figure 5: The mean absolute error and mean of the approximate upper bound $(\mathbf{w}^\top \mathbf{K}_0 \mathbf{w})^{1/2} (\mathbf{a}^\top \mathbf{K}_0 \mathbf{a})^{1/2}$, for different values of m in the sonar example of Section 3.3. Both are based on the semi-exact control functional method with $\Phi = \mathcal{P}^1$.

Theorem 1. *Let q be a probability density with $p/q > 0$ on \mathbb{R}^d . Let $V : \mathbb{R}^d \rightarrow [1, \infty)$. Consider a q -invariant, V -uniformly ergodic transition Markov chain $(\mathbf{x}^{(i)})_{i=1}^m$, such that*

- A1. $\sup_{\mathbf{x} \in \mathbb{R}^d} V(\mathbf{x})^{-r} k_0(\mathbf{x}, \mathbf{x})^2 < \infty$ for some $0 < r < 1$;
- A2. *the points $(\mathbf{x}^{(i)})_{i=1}^m$ are almost surely distinct and \mathcal{F} -unisolvent.*
- A3. $\limsup_{m \rightarrow \infty} \|\Pi \mathbf{1}\|_{\mathbf{K}_0^{-1}} / \|\mathbf{1}\|_{\mathbf{K}_0^{-1}} < 1$ *almost surely.*

Assume, in addition, that the hypotheses of Lemma 2 are satisfied and that

- A4. $|f|_{k_0, \mathcal{F}} < \infty$;

Then $I_{\text{SECF}}(f) \rightarrow I(f)$ in probability as $m \rightarrow \infty$.

The proof is provided in Appendix K. Assumption A1 serves to ensure that q is not too far removed from p , with respect to generating suitable states $\mathbf{x}^{(i)}$ for approximating integrals with respect to p , and are discussed in detail in Hodgkinson et al. (2020). Assumption A2 is used to ensure that the finite sample size bound (17) is well-defined. Assumption A3 ensures the points in the sequence $(\mathbf{x}^{(i)})_{i=1}^m$ distinguish (asymptotically) the constant function from the functions $\{\phi_i\}_{i=1}^{q-1}$, which is a weak technical requirement. Assumption A4 ensures a solution to the Stein equation, sufficient conditions for which are discussed in Mackey et al. (2016); Si et al. (2020).

5 Discussion

The problem of approximating posterior expectations is well-studied and powerful control variate and control functional methods exist to improve the accuracy of Monte Carlo integration. However, it is *a priori* unclear which of these methods

is most suitable for any given task. This paper demonstrates how both parametric and non-parametric approaches can be combined into a single estimator that remains competitive with the state-of-the-art in all regimes we considered. Moreover, we highlighted polynomial exactness in the Bernstein-von-Mises limit as a useful property that we believe can confer robustness of the estimator in a broad range of applied contexts. The multitude of applications for these methods, and their availability in the ZVCV package (South, 2020), suggests they are well-placed to have a practical impact.

Several possible extensions of the proposed method can be considered. For example, the parametric component Φ could be adapted to the particular f and p using a dimensionality reduction method. Likewise, extending cross-validation to encompass the choice of kernel and even the choice of control variate or control functional estimator may be useful. The potential for alternatives to the Nyström approximation to further improve scalability of the method can also be explored. In terms of the points $\mathbf{x}^{(i)}$ on which the estimator is defined, these could be optimally selected to minimize the error bound in (17), for example following the approaches of Chen et al. (2018, 2019). Finally, we highlight a possible extension to the case where only stochastic gradient information is available, following Friel et al. (2016) in the parametric context.

Acknowledgements CJO is grateful to Yvik Swan for discussion of Stein’s method. TK was supported by the Aalto ELEC Doctoral School and the Vilho, Yrjö and Kalle Väisälä Foundation. MG was supported by a Royal Academy of Engineering Research Chair and by the Engineering and Physical Sciences Research Council grants EP/T000414/1, EP/R018413/2, EP/P020720/2, EP/R034710/1, EP/R004889/1. TK, MG and CJO were supported by the Lloyd’s Register Foundation programme on data-centric engineering at the Alan Turing Institute, UK. CN and LFS were supported by the Engineering and Physical Sciences Research Council grants EP/S00159X/1 and EP/V022636/1. The authors are grateful for feedback from three anonymous Reviewers, an Associate Editor and an Editor, which led to an improved manuscript.

References

- Adams, R. A. and Fournier, J. J. (2003). *Sobolev Spaces*. Elsevier.
- Alaoui, A. and Mahoney, M. W. (2015). Fast randomized kernel ridge regression with statistical guarantees. In *Proceedings of the 29th Conference on Neural Information Processing Systems*, volume 28, pages 775–783.
- Assaraf, R. and Caffarel, M. (1999). Zero-variance principle for Monte Carlo algorithms. *Physical Review Letters*, 83(23):4682–4685.
- Barbour, A. D. (1988). Stein’s method and Poisson process convergence. *Journal of Applied Probability*, 25(A):175–184.

- Barp, A., Oates, C., Porcu, E., Girolami, M., et al. (2018). A Riemannian-Stein kernel method. *arXiv preprint arXiv:1810.04946*.
- Belkin, M., Hsu, D., Ma, S., and Mandal, S. (2019). Reconciling modern machine-learning practice and the classical bias–variance trade-off. *Proceedings of the National Academy of Sciences*, 116(32):15849–15854.
- Belomestny, D., Iosipoi, L., Moulines, E., Naumov, A., and Samsonov, S. (2019a). Variance reduction for Markov chains with application to MCMC. *arXiv preprint arXiv:1910.03643*.
- Belomestny, D., Iosipoi, L., and Zhivotovskiy, N. (2017). Variance reduction via empirical variance minimization: convergence and complexity. *arXiv preprint arXiv:1712.04667*.
- Belomestny, D., Moulines, E., Shagadatov, N., and Urusov, M. (2019b). Variance reduction for MCMC methods via martingale representations. *arXiv preprint arXiv:1903.07373*.
- Berlinet, A. and Thomas-Agnan, C. (2011). *Reproducing Kernel Hilbert Spaces in Probability and Statistics*. Springer Science & Business Media.
- Briol, F.-X., Oates, C. J., Girolami, M., Osborne, M. A., and Sejdinovic, D. (2019). Probabilistic integration: A role in statistical computation? (with discussion and rejoinder). *Statistical Science*, 34(1):1–22.
- Brosse, N., Durmus, A., Meyn, S., Éric Moulines, and Radhakrishnan, A. (2019). Diffusion approximations and control variates for MCMC. *arXiv preprint arXiv:1808.01665*.
- Chen, W. Y., Barp, A., Briol, F.-X., Gorham, J., Girolami, M., Mackey, L., Oates, C., et al. (2019). Stein point Markov chain Monte Carlo. In *Proceedings of the 36th International Conference on Machine Learning*.
- Chen, W. Y., Mackey, L., Gorham, J., Briol, F.-X., and Oates, C. J. (2018). Stein points. In *Proceedings of the 35th International Conference on Machine Learning*.
- Chopin, N. and Ridgway, J. (2017). Leave Pima Indians alone: binary regression as a benchmark for Bayesian computation. *Statistical Science*, 32(1):64–87.
- Chwialkowski, K., Strathmann, H., and Gretton, A. (2016). A kernel test of goodness of fit. In *Proceedings of the 33rd International Conference on Machine Learning*. JMLR: Workshop and Conference Proceedings.
- Clenshaw, C. W. and Curtis, A. R. (1960). A method for numerical integration on an automatic computer. *Numerische Mathematik*, 2(1):197–205.
- Dheeru, D. and Karra Taniskidou, E. (2017). UCI machine learning repository.
- Dick, J., Kuo, F. Y., and Sloan, I. H. (2013). High-dimensional integration: The quasi-Monte Carlo way. *Acta Numerica*, 22:133–288.

- Ermak, D. L. (1975). A computer simulation of charged particles in solution. I. Technique and equilibrium properties. *The Journal of Chemical Physics*, 62(10):4189–4196.
- Fasshauer, G. E. (2011). Positive-definite kernels: Past, present and future. *Dolomites Research Notes on Approximation*, 4:21–63.
- Fasshauer, G. E. and Ye, Q. (2011). Reproducing kernels of generalized Sobolev spaces via a Green function approach with distributional operators. *Numerische Mathematik*, 119(3):585–611.
- Friel, N., Mira, A., Oates, C. J., et al. (2016). Exploiting multi-core architectures for reduced-variance estimation with intractable likelihoods. *Bayesian Analysis*, 11(1):215–245.
- Garreau, D., Jitkrittum, W., and Kanagawa, M. (2017). Large sample analysis of the median heuristic. *arXiv preprint arXiv:1707.07269*.
- Gautschi, W. (2004). *Orthogonal Polynomials: Computation and Approximation*. Numerical Mathematics and Scientific Computation. Oxford University Press.
- Gorham, J. and Mackey, L. (2015). Measuring sample quality with Stein’s method. In *Proceedings of the 28th Conference on Neural Information Processing Systems*, volume 28, pages 226–234.
- Gorham, J. and Mackey, L. (2017). Measuring sample quality with kernels. In *Proceedings of the 34th International Conference on Machine Learning*, pages 1292–1301.
- Gorman, R. P. and Sejnowski, T. J. (1988). Analysis of hidden units in a layered network trained to classify sonar targets. *Neural Networks*, 1(1):75–89.
- Hammersley, J. M. and Handscomb, D. C. (1964). *Monte Carlo Methods*. Chapman & Hall.
- Hastings, W. K. (1970). Monte Carlo sampling methods using Markov chains and their applications. *Biometrika*, 57(1):97–109.
- Higham, N. J. (1988). Computing a nearest symmetric positive semidefinite matrix. *Linear Algebra and Its Applications*, 103:103–118.
- Hildebrand, F. B. (1987). *Introduction to Numerical Analysis*. Courier Corporation.
- Hodgkinson, L., Salomone, R., and Roosta, F. (2020). The reproducing Stein kernel approach for post-hoc corrected sampling. *arXiv preprint arXiv:2001.09266*.
- Karvonen, T., Oates, C. J., and Särkkä, S. (2018). A Bayes–Sard cubature method. In *Proceedings of the 32nd Conference on Neural Information Processing Systems*, volume 31, pages 5882–5893.

- Larkin, F. M. (1970). Optimal approximation in Hilbert spaces with reproducing kernel functions. *Mathematics of Computation*, 24(112):911–921.
- Larkin, F. M. (1974). Probabilistic error estimates in spline interpolation and quadrature. In *Information Processing 74: Proceedings of IFIP Congress 74*, pages 605–609. North-Holland.
- Lebreton, J. D., Burnham, K. P., Clobert, J., and Anderson, D. R. (1992). Modeling survival and testing biological hypotheses using marked animals: a unified approach with case studies. *Ecological Monographs*, 61(1):67–118.
- Liu, Q. and Lee, J. (2017). Black-box importance sampling. In *Proceedings of the 20th International Conference on Artificial Intelligence and Statistics*, pages 952–961.
- Liu, Q., Lee, J., and Jordan, M. (2016). A kernelized Stein discrepancy for goodness-of-fit tests. In *Proceedings of the 33rd International Conference on Machine Learning*, pages 276–284.
- Mackey, L., Gorham, J., et al. (2016). Multivariate Stein factors for a class of strongly log-concave distributions. *Electronic Communications in Probability*, 21(56).
- Marzolin, G. (1988). Polygynie du cincle plongeur (cinclus cinclus) dans le côtes de Lorraine. *Oiseau et la Revue Francaise d’Ornithologie*, 58(4):277–286.
- Meyn, S. P. and Tweedie, R. L. (1993). *Markov Chains and Stochastic Stability*. Springer-Verlag.
- Mijatović, A., Vogrinc, J., et al. (2018). On the Poisson equation for Metropolis–Hastings chains. *Bernoulli*, 24(3):2401–2428.
- Mira, A., Solgi, R., and Imparato, D. (2013). Zero variance Markov chain Monte Carlo for Bayesian estimators. *Statistics and Computing*, 23(5):653–662.
- Oates, C. J., Cockayne, J., Briol, F.-X., and Girolami, M. (2019). Convergence rates for a class of estimators based on Stein’s method. *Bernoulli*, 25(2):1141–1159.
- Oates, C. J., Girolami, M., and Chopin, N. (2017). Control functionals for Monte Carlo integration. *Journal of the Royal Statistical Society: Series B (Statistical Methodology)*, 79(3):695–718.
- Oates, C. J., Papamarkou, T., and Girolami, M. (2016). The controlled thermodynamic integral for Bayesian model evidence evaluation. *Journal of the American Statistical Association*, 111(514):634–645.
- Oettershagen, J. (2017). *Construction of Optimal Cubature Algorithms with Applications to Econometrics and Uncertainty Quantification*. PhD thesis, University of Bonn.

- O’Hagan, A. (1991). Bayes–Hermite quadrature. *Journal of Statistical Planning and Inference*, 29(3):245–260.
- Papamarkou, T., Mira, A., Girolami, M., et al. (2014). Zero variance differential geometric Markov chain Monte Carlo algorithms. *Bayesian Analysis*, 9(1):97–128.
- Parisi, G. (1981). Correlation functions and computer simulations. *Nuclear Physics B*, 180(3):378–384.
- Ripley, B. (1987). *Stochastic Simulation*. John Wiley & Sons.
- Robert, C. and Casella, G. (2013). *Monte Carlo Statistical Methods*. Springer Science & Business Media.
- Roberts, G. O., Tweedie, R. L., et al. (1996). Exponential convergence of Langevin distributions and their discrete approximations. *Bernoulli*, 2(4):341–363.
- Rudi, A., Camoriano, R., and Rosasco, L. (2015). Less is more: Nyström computational regularization. In *Proceedings of the 29th Conference on Neural Information Processing Systems*, pages 1657–1665.
- Rudi, A., Carratino, L., and Rosasco, L. (2017). FALKON: An optimal large scale kernel method. In *Proceedings of the 31st Conference on Neural Information Processing Systems*, pages 3888–3898.
- Sard, A. (1949). Best approximate integration formulas; best approximation formulas. *American Journal of Mathematics*, 71(1):80–91.
- Si, S., Oates, C. J., Duncan, A. B., Carin, L., and Briol, F.-X. (2020). Scalable control variates for monte carlo methods via stochastic optimization. *arXiv*.
- Singhal, R., Lahlou, S., and Ranganath, R. (2019). Kernelized complete conditional Stein discrepancy. *arXiv preprint arXiv:1904.04478*.
- Smola, A. J. and Schölkopf, B. (2000). Sparse greedy matrix approximation for machine learning. In *Proceedings of the 17th International Conference on Machine Learning*.
- South, L. F. (2020). *ZVCV: Zero-Variance Control Variates*. R package version 2.1.0.
- South, L. F., Oates, C. J., Mira, A., and Drovandi, C. (2019). Regularised zero-variance control variates for high-dimensional variance reduction. *arXiv preprint arXiv:1811.05073*.
- Stein, C. (1972). A bound for the error in the normal approximation to the distribution of a sum of dependent random variables. In *Proceedings of the 6th Berkeley Symposium on Mathematical Statistics and Probability*, volume 2, pages 583–602. University of California Press.

- Steinwart, I. and Christmann, A. (2008). *Support Vector Machines*. Information Science and Statistics. Springer.
- van der Vaart, A. (1998). *Asymptotic Statistics*. Cambridge series on statistical and probabilistic mathematics. Cambridge University Press.
- Wahba, G. (1990). *Spline Models for Observational Data*. Number 59 in CBMS-NSF Regional Conference Series in Applied Mathematics. Society for Industrial and Applied Mathematics.
- Wan, R., Zhong, M., Xiong, H., and Zhu, Z. (2019). Neural control variates for variance reduction. In *European Conference on Machine Learning and Principles and Practice of Knowledge Discovery in Databases*.
- Wendland, H. (2004). *Scattered Data Approximation*, volume 17. Cambridge university press.
- Williams, C. K. I. and Seeger, M. (2001). Using the Nyström method to speed up kernel machines. In *Proceedings of the 14th Conference on Neural Information Processing Systems*, pages 682–688.

Supplementary Material

A Proof of Lemma 1

Lemmas 1 and 2 are stylised versions of similar results that can be found in earlier work, such as Chwialkowski et al. (2016); Liu et al. (2016); Oates et al. (2017). Our presentation differs in that we provide a convenient explicit sufficient condition, on the tails of $\|\nabla g\|$ for Lemma 1, and on the tails of $\|\nabla_{\mathbf{x}} \nabla_{\mathbf{y}}^{\top} k(\mathbf{x}, \mathbf{y})\|$ and $\|\nabla_{\mathbf{x}} \Delta_{\mathbf{y}} k(\mathbf{x}, \mathbf{y})\|$ for Lemma 2, for their conclusions to hold.

Proof. The stated assumptions on the differentiability of p and g imply that the vector field $p(\mathbf{x}) \nabla_{\mathbf{x}} g(\mathbf{x})$ is continuously differentiable on \mathbb{R}^d . The divergence theorem can therefore be applied, over any compact set $D \subset \mathbb{R}^d$ with piecewise smooth boundary ∂D , to reveal that

$$\begin{aligned} \int_D (\mathcal{L}g)(\mathbf{x}) p(\mathbf{x}) d\mathbf{x} &= \int_D [\Delta_{\mathbf{x}} g(\mathbf{x}) + \nabla_{\mathbf{x}} g(\mathbf{x}) \cdot \nabla_{\mathbf{x}} \log p(\mathbf{x})] p(\mathbf{x}) d\mathbf{x} \\ &= \int_D \left[\frac{1}{p(\mathbf{x})} \nabla_{\mathbf{x}} \cdot (p(\mathbf{x}) \nabla_{\mathbf{x}} g(\mathbf{x})) \right] p(\mathbf{x}) d\mathbf{x} \\ &= \int_D \nabla_{\mathbf{x}} \cdot (p(\mathbf{x}) \nabla_{\mathbf{x}} g(\mathbf{x})) d\mathbf{x} \\ &= \oint_{\partial D} p(\mathbf{x}) \nabla_{\mathbf{x}} g(\mathbf{x}) \cdot \mathbf{n}(\mathbf{x}) \sigma(d\mathbf{x}), \end{aligned}$$

where $\mathbf{n}(\mathbf{x})$ is the unit normal vector at $\mathbf{x} \in \partial D$ and $\sigma(d\mathbf{x})$ is the surface element at $\mathbf{x} \in \partial D$. Next, we let $D = D_R = \{\mathbf{x} : \|\mathbf{x}\| \leq R\}$ be the ball in \mathbb{R}^d with radius R , so that ∂D_R is the sphere $S_R = \{\mathbf{x} : \|\mathbf{x}\| = R\}$. The assumption $\|\nabla_{\mathbf{x}} g(\mathbf{x})\| \leq C \|\mathbf{x}\|^{-\delta} p(\mathbf{x})^{-1}$ in the statement of the lemma allows us to establish the bound

$$\begin{aligned} \left| \oint_{S_R} p(\mathbf{x}) \nabla_{\mathbf{x}} g(\mathbf{x}) \cdot \mathbf{n}(\mathbf{x}) \sigma(d\mathbf{x}) \right| &\leq \oint_{S_R} |p(\mathbf{x}) \nabla_{\mathbf{x}} g(\mathbf{x}) \cdot \mathbf{n}(\mathbf{x})| \sigma(d\mathbf{x}) \leq \oint_{S_R} p(\mathbf{x}) \|\nabla_{\mathbf{x}} g(\mathbf{x})\| \sigma(d\mathbf{x}) \\ &\leq \oint_{S_R} C \|\mathbf{x}\|^{-\delta} \sigma(d\mathbf{x}) \\ &= CR^{-\delta} \oint_{S_R} \sigma(d\mathbf{x}) \\ &= CR^{-\delta} \frac{2\pi^{d/2}}{\Gamma(d/2)} R^{d-1}, \end{aligned}$$

where in the first and second inequalities we used Jensen's inequality and Cauchy-Schwarz, respectively, and in the final equality we have made use of the surface area of S_R . The assumption that $\delta > d - 1$ is then sufficient to obtain the result:

$$\left| \int (\mathcal{L}g)(\mathbf{x}) p(\mathbf{x}) d\mathbf{x} \right| = \lim_{R \rightarrow \infty} \left| \oint_{S_R} p(\mathbf{x}) \nabla_{\mathbf{x}} g(\mathbf{x}) \cdot \mathbf{n}(\mathbf{x}) \sigma(d\mathbf{x}) \right| \leq \lim_{R \rightarrow \infty} C \frac{2\pi^{d/2}}{\Gamma(d/2)} R^{d-1-\delta} = 0.$$

This completes the argument. \square

B Differentiating the Kernel

This appendix provides explicit forms of (8) for kernels k that are radial. First we present a generic result in Lemma 5 before specialising to the cases of the rational quadratic (Section B.1), Gaussian (Section B.2) and Matérn (Section B.3) kernels.

Lemma 5. *Consider a radial kernel k , meaning that k has the form*

$$k(\mathbf{x}, \mathbf{y}) = \Psi(z), \quad z = \|\mathbf{x} - \mathbf{y}\|^2,$$

where the function $\Psi: [0, \infty) \rightarrow \mathbb{R}$ is four times differentiable and $\mathbf{x}, \mathbf{y} \in \mathbb{R}^d$. Then (8) simplifies to

$$\begin{aligned} k_0(\mathbf{x}, \mathbf{y}) = & 16z^2\Psi^{(4)}(z) + 16(2+d)z\Psi^{(3)}(z) + 4(2+d)d\Psi^{(2)}(z) \\ & + 4[2z\Psi^{(3)}(z) + (2+d)\Psi^{(2)}(z)][\mathbf{u}(\mathbf{x}) - \mathbf{u}(\mathbf{y})]^\top(\mathbf{x} - \mathbf{y}) \\ & - 4\Psi^{(2)}(z)\mathbf{u}(\mathbf{x})^\top(\mathbf{x} - \mathbf{y})(\mathbf{x} - \mathbf{y})^\top\mathbf{u}(\mathbf{y}) - 2\Psi^{(1)}(z)\mathbf{u}(\mathbf{x})^\top\mathbf{u}(\mathbf{y}), \end{aligned} \quad (18)$$

where $\mathbf{u}(\mathbf{x}) = \nabla_{\mathbf{x}} \log p(\mathbf{x})$.

Proof. The proof is direct and based on have the following applications of the chain rule:

$$\begin{aligned} \nabla_{\mathbf{x}} k(\mathbf{x}, \mathbf{y}) &= 2\Psi^{(1)}(z)(\mathbf{x} - \mathbf{y}), \\ \nabla_{\mathbf{y}} k(\mathbf{x}, \mathbf{y}) &= -2\Psi^{(1)}(z)(\mathbf{x} - \mathbf{y}), \\ \Delta_{\mathbf{x}} k(\mathbf{x}, \mathbf{y}) &= 4z\Psi^{(2)}(z) + 2d\Psi^{(1)}(z), \\ \Delta_{\mathbf{y}} k(\mathbf{x}, \mathbf{y}) &= 4z\Psi^{(2)}(z) + 2d\Psi^{(1)}(z), \\ \partial_{x_i}\partial_{y_j} k(\mathbf{x}, \mathbf{y}) &= -4\Psi^{(2)}(z)(x_i - y_i)(x_j - y_j) - 2\Psi^{(1)}(z)\delta_{ij}, \\ \nabla_{\mathbf{x}}\Delta_{\mathbf{y}} k(\mathbf{x}, \mathbf{y}) &= 8z\Psi^{(3)}(z)(\mathbf{x} - \mathbf{y}) + 4(2+d)\Psi^{(2)}(z)(\mathbf{x} - \mathbf{y}), \\ \nabla_{\mathbf{y}}\Delta_{\mathbf{x}} k(\mathbf{x}, \mathbf{y}) &= -8z\Psi^{(3)}(z)(\mathbf{x} - \mathbf{y}) - 4(2+d)\Psi^{(2)}(z)(\mathbf{x} - \mathbf{y}), \\ \Delta_{\mathbf{x}}\Delta_{\mathbf{y}} k(\mathbf{x}, \mathbf{y}) &= 16z^2\Psi^{(4)}(z) + 16(2+d)z\Psi^{(3)}(z) + 4(2+d)d\Psi^{(2)}(z). \end{aligned}$$

Upon insertion of these formulae into (8), the desired result is obtained. \square

Thus for kernels that are radial, it is sufficient to compute just the derivatives $\Psi^{(j)}$ of the radial part.

B.1 Rational Quadratic Kernel

The rational quadratic kernel,

$$\Psi(z) = (1 + \lambda^{-2}z)^{-1},$$

has derivatives $\Psi^{(j)}(z) = (-1)^j \lambda^{-2j} j! (1 + \lambda^{-2}z)^{-j-1}$ for $j \geq 1$.

B.2 Gaussian Kernel

For the Gaussian kernel we have $\Psi(z) = \exp(-z/\lambda^2)$. Consequently,

$$\Psi^{(j)}(z) = (-1)^j \lambda^{-2j} \exp(-z/\lambda^2),$$

for $j \geq 1$.

B.3 Matérn Kernels

For a Matérn kernel of smoothness $\nu > 0$ we have

$$\Psi(z) = bc^\nu z^{\nu/2} K_\nu(c\sqrt{z}), \quad b = \frac{2^{1-\nu}}{\Gamma(\nu)}, \quad c = \frac{\sqrt{2\nu}}{\lambda},$$

where Γ the Gamma function and K_ν the modified Bessel function of the second kind of order ν . By the use of the formula $\partial_z K_\nu(z) = -K_{\nu-1}(z) - \frac{\nu}{z}K_\nu(z)$ we obtain

$$\Psi^{(j)}(z) = (-1)^j \frac{bc^{\nu+j}}{2^j} z^{(\nu-j)/2} K_{\nu-j}(c\sqrt{z}),$$

for $j = 1, \dots, 4$. In order to guarantee that the kernel is twice continuously differentiable, so that k_0 in (7) is well-defined, we require that $\lceil \nu \rceil > 2$. As a Matérn kernel induces a reproducing kernel Hilbert space that is norm-equivalent to the standard Sobolev space of order $\nu + \frac{d}{2}$ (Fasshauer and Ye, 2011, Example 5.7), the condition $\lceil \nu \rceil > 2$ implies, by the Sobolev imbedding theorem (Adams and Fournier, 2003, Theorem 4.12), that the functions in $\mathcal{G}(k)$ are twice continuously differentiable. Notice that $\Psi^{(3)}(z)$ and $\Psi^{(4)}(z)$ may not be defined at $z = 0$, in which case the terms $16z^2\Psi^{(4)}(z)$, $16(2+d)z\Psi^{(3)}(z)$ and $8z\Psi^{(3)}(z)$ in (18) must be interpreted as limits as $z \rightarrow 0$ from the right.

C Properties of $\mathcal{H} = \mathcal{G}(k_0)$

The purpose of this appendix is to establish basic properties of the reproducing kernel Hilbert space $\mathcal{H} = \mathcal{G}(k_0)$ of the kernel k_0 in (7). In Lemma 6 we clarify the reproducing kernel Hilbert space structure of \mathcal{H} . Then in Lemma 7 we establish square integrability of the elements of \mathcal{H} and in Lemma 8 we establish the local smoothness of the elements of \mathcal{H} .

To state these results we require several items of notation: The notation $C^s(\mathbb{R}^d)$ denotes the set of s -times continuously differentiable functions on \mathbb{R}^d ; i.e. $\partial^\alpha f \in C^0(\mathbb{R}^d)$ for all $|\alpha| \leq s$ where $C^0(\mathbb{R}^d)$ denotes the set of continuous functions on \mathbb{R}^d . For two normed spaces V and W , let $V \hookrightarrow W$ denote that V is continuously embedded in W , meaning that $\|v\|_W \leq C\|v\|_V$ for all $v \in V$ and some constant $C \geq 0$. In particular, we write $V \simeq W$ if and only if V and W are equal as sets and both $V \hookrightarrow W$ and $W \hookrightarrow V$. Let $\mathcal{L}^2(p)$ denote the vector space of square integrable functions with respect to p and equip this with the norm $\|h\|_{\mathcal{L}^2(p)} = (\int h(\mathbf{x})^2 p(\mathbf{x}) d\mathbf{x})^{1/2}$. For $h : \mathbb{R}^d \rightarrow \mathbb{R}$ and $D \subset \mathbb{R}^d$ we let $h|_D : D \rightarrow \mathbb{R}$ denote the restriction of h to D .

First we clarify the reproducing kernel Hilbert space structure of \mathcal{H} :

Lemma 6 (Reproducing kernel Hilbert space structure of \mathcal{H}). *Let $k : \mathbb{R}^d \times \mathbb{R}^d \rightarrow \mathbb{R}$ be a positive-definite kernel such that the regularity assumptions of Lemma 2 are satisfied. Let \mathcal{H} denote the normed space of real-valued functions on \mathbb{R}^d with norm*

$$\|h\|_{\mathcal{H}} = \inf_{\substack{h = \mathcal{L}g \\ g \in \mathcal{G}(k)}} \|g\|_{\mathcal{G}(k)}.$$

Then \mathcal{H} admits the structure of a reproducing kernel Hilbert space with kernel $\kappa : \mathbb{R}^d \times \mathbb{R}^d \rightarrow \mathbb{R}$ given by $\kappa(\mathbf{x}, \mathbf{y}) = k_0(\mathbf{x}, \mathbf{y})$. That is, $\mathcal{H} = \mathcal{G}(k_0)$. Moreover, for $D \neq \emptyset$, let $\mathcal{H}|_D$ denote the normed space of real-valued functions on D with norm

$$\|h'\|_{\mathcal{H}|_D} = \inf_{\substack{h|_D=h' \\ h \in \mathcal{H}}} \|h\|_{\mathcal{H}}.$$

Then $\mathcal{H}|_D$ is a reproducing kernel Hilbert space with kernel $\kappa|_D : D \times D \rightarrow \mathbb{R}$ given by $\kappa|_D(\mathbf{x}, \mathbf{y}) = k_0(\mathbf{x}, \mathbf{y})$. That is, $\mathcal{H}|_D = \mathcal{G}(\kappa|_D)$.

Proof. The first statement is an immediate consequence of Theorem 5 in Section 4.1 of Berlinet and Thomas-Agnan (2011). The second statement is an immediate consequence of Theorem 6 in Section 4.2 of Berlinet and Thomas-Agnan (2011). \square

Next we establish when the elements of \mathcal{H} are square-integrable functions with respect to p .

Lemma 7 (Square integrability of \mathcal{H}). *Let κ be a radial kernel satisfying the pre-conditions of Lemma 5. If $u_i = \nabla_{x_i} \log p(\mathbf{x}) \in \mathcal{L}^2(p)$ for each $i = 1, \dots, d$, then $\mathcal{H} \hookrightarrow \mathcal{L}^2(p)$.*

Proof. From the representer theorem and Cauchy–Schwarz we have that

$$\int h(\mathbf{x})^2 p(\mathbf{x}) d\mathbf{x} = \int \langle h, \kappa(\cdot, \mathbf{x}) \rangle_{\mathcal{H}}^2 p(\mathbf{x}) d\mathbf{x} \leq \|h\|_{\mathcal{H}}^2 \int \kappa(\mathbf{x}, \mathbf{x}) p(\mathbf{x}) d\mathbf{x}. \quad (19)$$

Now, in the special case $k(\mathbf{x}, \mathbf{y}) = \Psi(z)$, $z = \|\mathbf{x} - \mathbf{y}\|^2$, the conclusion of Lemma 5 gives that $\kappa(\mathbf{x}, \mathbf{x}) = 4(2 + d)d\Psi^{(2)}(0) - 2\Psi^{(1)}(0)\|\mathbf{u}(\mathbf{x})\|^2$, from which it follows that

$$0 \leq \int \kappa(\mathbf{x}, \mathbf{x}) p(\mathbf{x}) d\mathbf{x} = 4(2 + d)d\Psi^{(2)}(0) - 2\Psi^{(1)}(0) \int \|\mathbf{u}(\mathbf{x})\|^2 p(\mathbf{x}) d\mathbf{x} = C^2. \quad (20)$$

The combination of (19) and (20) establishes that $\|h\|_{\mathcal{L}^2(p)} \leq C\|h\|_{\mathcal{H}}$, which is the claimed result. \square

Finally we turn to the regularity of the elements of \mathcal{H} , as quantified by their smoothness over suitable bounded sets $D \subset \mathbb{R}^d$. In what follows we will let $\mathcal{G}(k)$ be a reproducing kernel Hilbert space of functions in $\mathcal{L}^2(\mathbb{R}^d)$, the space of square Lebesgue integrable functions on \mathbb{R}^d , such that the norms

$$\|h\|_{\mathcal{G}(k)} \simeq \|h\|_{W_2^r(\mathbb{R}^d)} = \left(\sum_{|\alpha| \leq r} \|\partial^\alpha h\|_{\mathcal{L}^2(\mathbb{R}^d)}^2 \right)^{\frac{1}{2}}$$

are equivalent. The latter is recognized as the standard Sobolev norm; this space is denoted $W_2^r(\mathbb{R}^d)$. For example, the Matérn kernel in Section B.3 corresponds to $\mathcal{G}(k)$ with $r = \nu + \frac{d}{2}$. The Sobolev embedding theorem implies that $W_2^r(\mathbb{R}^d) \subset C^0(\mathbb{R}^d)$ whenever $r > \frac{d}{2}$.

The following result establishes the smoothness of \mathcal{H} in terms of the differentiability of its elements. If the smoothness of f is known then k should be selected so that the smoothness of \mathcal{H} matches it.

Lemma 8 (Smoothness of \mathcal{H}). *Let $r, s \in \mathbb{N}$ be such that $r > s + 2 + \frac{d}{2}$. If $\mathcal{G}(k) \simeq W_2^r(\mathbb{R}^d)$ and $\log p \in C^{s+1}(\mathbb{R}^d)$, then, for any open and bounded set $D \subset \mathbb{R}^d$, we have $\mathcal{H}|_D \hookrightarrow W_2^s(D)$.*

Proof. Under our assumptions, the kernel $\kappa|_D : D \times D \rightarrow \mathbb{R}$ from Lemma 6 is s -times continuously differentiable in the sense of Definition 4.35 of Steinwart and Christmann (2008). It follows from Lemma 4.34 of Steinwart and Christmann (2008) that $\partial_{\mathbf{x}}^{\alpha} \kappa|_D(\cdot, \mathbf{x}) \in \mathcal{H}|_D$ for all $\mathbf{x} \in D$ and $|\alpha| \leq s$. From the reproducing property in $\mathcal{H}|_D$ and the Cauchy–Schwarz inequality we have that, for $|\alpha| \leq s$,

$$|\partial^{\alpha} f(\mathbf{x})| = |\langle f, \partial^{\alpha} \kappa|_D(\cdot, \mathbf{x}) \rangle_{\mathcal{H}|_D}| \leq \|f\|_{\mathcal{H}|_D} \|\partial^{\alpha} \kappa|_D(\cdot, \mathbf{x})\|_{\mathcal{H}|_D} = \|f\|_{\mathcal{H}|_D} \left(\partial_{\mathbf{x}}^{\alpha} \partial_{\mathbf{y}}^{\alpha} \kappa|_D(\mathbf{x}, \mathbf{y})|_{\mathbf{y}=\mathbf{x}} \right)^{1/2}.$$

See also Corollary 4.36 of Steinwart and Christmann (2008). Thus it follows from the definition of $W_2^s(D)$ and the reproducing property that

$$\begin{aligned} \|f\|_{W_2^s(D)}^2 &= \sum_{|\alpha| \leq s} \|\partial^{\alpha} f\|_{L_2(D)}^2 \leq \|f\|_{\mathcal{H}|_D}^2 \sum_{|\alpha| \leq s} \|\mathbf{x} \mapsto \partial_{\mathbf{x}}^{\alpha} \partial_{\mathbf{y}}^{\alpha} \kappa|_D(\mathbf{x}, \mathbf{y})|_{\mathbf{y}=\mathbf{x}}\|_{L_2(D)}^2 \\ &= \|f\|_{\mathcal{H}|_D}^2 \|\mathbf{x} \mapsto \kappa|_D(\mathbf{x}, \mathbf{x})\|_{W_2^s(D)}^2. \end{aligned}$$

Now, from the definition of κ and using the fact that k is symmetric, we have that

$$\kappa(\mathbf{x}, \mathbf{x}) = \Delta_{\mathbf{x}} \Delta_{\mathbf{y}} k(\mathbf{x}, \mathbf{y})|_{\mathbf{y}=\mathbf{x}} + 2\mathbf{u}(\mathbf{x})^{\top} \nabla_{\mathbf{x}} \Delta_{\mathbf{y}} k(\mathbf{x}, \mathbf{y})|_{\mathbf{y}=\mathbf{x}} + \mathbf{u}(\mathbf{x})^{\top} [\nabla_{\mathbf{x}} \nabla_{\mathbf{y}}^{\top} k(\mathbf{x}, \mathbf{y})|_{\mathbf{y}=\mathbf{x}}] \mathbf{u}(\mathbf{x}).$$

Our assumption that $\mathcal{G}(k) \simeq W_2^r(\mathbb{R}^d)$ with $r > s + 2 + \frac{d}{2}$ implies that each of the functions $\mathbf{x} \mapsto \Delta_{\mathbf{x}} \Delta_{\mathbf{y}} k(\mathbf{x}, \mathbf{y})|_{\mathbf{y}=\mathbf{x}}$, $\nabla_{\mathbf{x}} \Delta_{\mathbf{y}} k(\mathbf{x}, \mathbf{y})|_{\mathbf{y}=\mathbf{x}}$ and $\nabla_{\mathbf{x}} \nabla_{\mathbf{y}}^{\top} k(\mathbf{x}, \mathbf{y})|_{\mathbf{y}=\mathbf{x}}$, are $C^s(\mathbb{R}^d)$. In addition, our assumption that $\log p \in C^{s+1}(\mathbb{R}^d)$ implies that $\mathbf{x} \mapsto \mathbf{u}(\mathbf{x}) \in C^s(\mathbb{R}^d)$. Thus $\mathbf{x} \mapsto \kappa(\mathbf{x}, \mathbf{x})$ is $C^s(\mathbb{R}^d)$ and in particular the boundedness of D implies that $\|\mathbf{x} \mapsto \kappa|_D(\mathbf{x}, \mathbf{x})\|_{W_2^s(D)} < \infty$ as required. \square

D Proof of Lemma 2

Proof. In what follows C is a generic positive constant, independent of \mathbf{x} but possibly dependant on \mathbf{y} , whose value can differ each time it is instantiated. The aim of this proof is to apply Lemma 1 to the function $g(\mathbf{x}) = \mathcal{L}_{\mathbf{y}} k(\mathbf{x}, \mathbf{y})$. Our task is to verify the pre-condition $\|\nabla_{\mathbf{x}} g(\mathbf{x})\| \leq C \|\mathbf{x}\|^{-\delta} p(\mathbf{x})^{-1}$ for some $\delta > d - 1$. It will then follow from the conclusion of Lemma 1 that $\int k_0(\mathbf{x}, \mathbf{y}) p(\mathbf{x}) d\mathbf{x} = 0$ as required. To this end, expanding the term $\|\nabla_{\mathbf{x}} g(\mathbf{x})\|^2$, we have that

$$\begin{aligned} \|\nabla_{\mathbf{x}} g(\mathbf{x})\|^2 &= \|\nabla_{\mathbf{x}} \mathcal{L}_{\mathbf{y}} k(\mathbf{x}, \mathbf{y})\|^2 \\ &= \|\nabla_{\mathbf{x}} \Delta_{\mathbf{y}} k(\mathbf{x}, \mathbf{y}) + \nabla_{\mathbf{x}} [\nabla_{\mathbf{y}} \log p(\mathbf{y}) \cdot \nabla_{\mathbf{y}} k(\mathbf{x}, \mathbf{y})]\|^2 \\ &= \|\nabla_{\mathbf{x}} \Delta_{\mathbf{y}} k(\mathbf{x}, \mathbf{y})\|^2 + 2\nabla_{\mathbf{x}} [\nabla_{\mathbf{y}} \log p(\mathbf{y}) \cdot \nabla_{\mathbf{y}} k(\mathbf{x}, \mathbf{y})]^{\top} \nabla_{\mathbf{x}} \Delta_{\mathbf{y}} k(\mathbf{x}, \mathbf{y}) \\ &\quad + \|\nabla_{\mathbf{x}} [\nabla_{\mathbf{y}} \log p(\mathbf{y}) \cdot \nabla_{\mathbf{y}} k(\mathbf{x}, \mathbf{y})]\|^2 \\ &= \|\nabla_{\mathbf{x}} \Delta_{\mathbf{y}} k(\mathbf{x}, \mathbf{y})\|^2 + 2\{[\nabla_{\mathbf{x}} \nabla_{\mathbf{y}}^{\top} k(\mathbf{x}, \mathbf{y})]^{\top} \nabla_{\mathbf{y}} \log p(\mathbf{y})\}^{\top} \nabla_{\mathbf{x}} \Delta_{\mathbf{y}} k(\mathbf{x}, \mathbf{y}) \\ &\quad + \|\nabla_{\mathbf{x}} \nabla_{\mathbf{y}}^{\top} k(\mathbf{x}, \mathbf{y}) \nabla_{\mathbf{y}} \log p(\mathbf{y})\|^2 \end{aligned}$$

$$\begin{aligned} &\leq \|\nabla_{\mathbf{x}} \Delta_{\mathbf{y}} k(\mathbf{x}, \mathbf{y})\|^2 + 2\|[\nabla_{\mathbf{x}} \nabla_{\mathbf{y}}^\top k(\mathbf{x}, \mathbf{y})]^\top \nabla_{\mathbf{y}} \log p(\mathbf{y})\| \|\nabla_{\mathbf{x}} \Delta_{\mathbf{y}} k(\mathbf{x}, \mathbf{y})\| \\ &\quad + \|[\nabla_{\mathbf{x}} \nabla_{\mathbf{y}}^\top k(\mathbf{x}, \mathbf{y})] \nabla_{\mathbf{y}} \log p(\mathbf{y})\|^2 \end{aligned} \quad (21)$$

$$\begin{aligned} &\leq \|\nabla_{\mathbf{x}} \Delta_{\mathbf{y}} k(\mathbf{x}, \mathbf{y})\|^2 + 2\|\nabla_{\mathbf{x}} \nabla_{\mathbf{y}}^\top k(\mathbf{x}, \mathbf{y})\|_{\text{OP}} \|\nabla_{\mathbf{y}} \log p(\mathbf{y})\| \|\nabla_{\mathbf{x}} \Delta_{\mathbf{y}} k(\mathbf{x}, \mathbf{y})\| \\ &\quad + \|\nabla_{\mathbf{x}} \nabla_{\mathbf{y}}^\top k(\mathbf{x}, \mathbf{y})\|_{\text{OP}}^2 \|\nabla_{\mathbf{y}} \log p(\mathbf{y})\|^2 \end{aligned} \quad (22)$$

$$\begin{aligned} &\leq [C\|\mathbf{x}\|^{-\delta} p(\mathbf{x})^{-1}]^2 + 2[C\|\mathbf{x}\|^{-\delta} p(\mathbf{x})^{-1}] \|\nabla_{\mathbf{y}} \log p(\mathbf{y})\| [C\|\mathbf{x}\|^{-\delta} p(\mathbf{x})^{-1}] \\ &\quad + [C\|\mathbf{x}\|^{-\delta} p(\mathbf{x})^{-1}]^2 \|\nabla_{\mathbf{y}} \log p(\mathbf{y})\|^2 \end{aligned} \quad (23)$$

$$\leq C\|\mathbf{x}\|^{-2\delta} p(\mathbf{x})^{-2}$$

as required. Here (21) follows from the Cauchy–Schwarz inequality applied to the second term, (22) follows from the definition of the operator norm $\|\cdot\|_{\text{OP}}$ and (23) employs the pre-conditions that we have assumed. \square

E Proof of Lemma 3

Proof. Our first task is to establish that it is sufficient to prove the result in just the particular case $\hat{\mathbf{x}}_n = \mathbf{0}$ and $n^{-1}I(\hat{\mathbf{x}}_n)^{-1} = \mathbf{I}$, where \mathbf{I} is the d -dimensional identity matrix. Indeed, if $\hat{\mathbf{x}}_n \neq \mathbf{0}$ or $n^{-1}I(\hat{\mathbf{x}}_n)^{-1} \neq \mathbf{I}$, then let $\mathbf{t}(\mathbf{x}) = \mathbf{W}(\mathbf{x} - \hat{\mathbf{x}}_n)$ where \mathbf{W} is a non-singular matrix satisfying $\mathbf{W}^\top \mathbf{W} = nI(\hat{\mathbf{x}}_n)$ so that $\mathbf{t}(\mathbf{x}) \sim \mathcal{N}(\mathbf{0}, \mathbf{I})$. Under the same co-ordinate transformation the polynomial subspace

$$A = \mathcal{P}_0^r = \text{span}\{\mathbf{x}^\alpha : \alpha \in \mathbb{N}_0^d, 0 \leq |\alpha| \leq r\}$$

becomes $B = \text{span}\{\mathbf{t}(\mathbf{x})^\alpha : \alpha \in \mathbb{N}_0^d, 0 \leq |\alpha| \leq r\}$. Exact integration of functions in A with respect to $\mathcal{N}(\hat{\mathbf{x}}_n, \mathbf{I})$ corresponds to exact integration of functions in B with respect to $\mathcal{N}(\mathbf{0}, \mathbf{I})$. Thus our first task is to establish that $B = A$. Clearly B is a linear subspace of A , since elements of B can be expanded out into monomials and monomials generate A , so it remains to argue that B is all of A . In what follows we will show that $\dim(B) = \dim(A)$ and this will complete the first part of the argument.

The co-ordinate transform \mathbf{t} is an invertible affine map on \mathbb{R}^d . The action of such a map \mathbf{t} on a set S of functions on \mathbb{R}^d can be defined as $\mathbf{t}(S) = \{\mathbf{x} \rightarrow s(\mathbf{t}(\mathbf{x})) : s \in S\}$. Thus $B = \mathbf{t}(A)$. Let $\mathbf{t}^*(\mathbf{x}) = \mathbf{W}^{-1}\mathbf{x} + \hat{\mathbf{x}}_n$ and notice that this is also an invertible affine map on \mathbb{R}^d with $\mathbf{t}^*(\mathbf{t}(\mathbf{x})) = \mathbf{x}$ being the identity map on \mathbb{R}^d . The composition of invertible affine maps on \mathbb{R}^d is again an invertible affine map and thus $\mathbf{t}^*\mathbf{t}$ is also an invertible affine map on \mathbb{R}^d and its action on a set is well-defined. Considering the action of $\mathbf{t}^*\mathbf{t}$ on the set A gives that $\mathbf{t}^*(\mathbf{t}(A)) = A$ and therefore $\mathbf{t}(A)$ must have the same dimension as A . Thus $\dim(A) = \dim(\mathbf{t}(A)) = \dim(B)$ as claimed.

Our second task is to show that, in the case where p is the density of $\mathcal{N}(\mathbf{0}, \mathbf{I})$ and thus $\nabla_{\mathbf{x}} \log p(\mathbf{x}) = -\mathbf{x}$, the set $\mathcal{F} = \text{span}\{1\} \oplus \mathcal{LP}^r$ on which I_{CV} is exact is equal to \mathcal{P}_0^r . Our proof proceeds by induction on the maximal degree r of the polynomial. For the base case we take $r = 1$:

$$\text{span}\{1\} \oplus \mathcal{LP}^1 = \text{span}\{1\} \oplus \text{span}\{\mathcal{L}x_j : j = 1, \dots, d\}$$

$$\begin{aligned}
&= \text{span}\{1\} \oplus \text{span}\{\Delta_{\mathbf{x}}x_j + \nabla_{\mathbf{x}} \log p(\mathbf{x}) \cdot \nabla_{\mathbf{x}}(x_j) : j = 1, \dots, d\} \\
&= \text{span}\{1\} \oplus \text{span}\{0 - \mathbf{x} \cdot \mathbf{e}_j : j = 1, \dots, d\} \\
&= \text{span}\{1\} \oplus \text{span}\{-x_j : j = 1, \dots, d\} \\
&= \mathcal{P}_0^1.
\end{aligned}$$

For the inductive step we assume that $\text{span}\{1\} \oplus \mathcal{LP}^{r-1} = \mathcal{P}_0^{r-1}$ holds for a given $r \geq 2$ and aim to show that $\text{span}\{1\} \oplus \mathcal{LP}^r = \mathcal{P}_0^r$. Note that the action of \mathcal{L} on a polynomial of order r will return a polynomial of order at most r , so that $\text{span}\{1\} \oplus \mathcal{LP}^r \subseteq \mathcal{P}_0^r$ and thus we need to show that $\mathcal{P}_0^r \subseteq \text{span}\{1\} \oplus \mathcal{LP}^r$. Under the inductive assumption we have that

$$\begin{aligned}
\text{span}\{1\} \oplus \mathcal{LP}^r &= \text{span}\{1\} \oplus \left(\mathcal{LP}^{r-1} \oplus \text{span}\{\mathcal{L}\mathbf{x}^\alpha : \alpha \in \mathbb{N}_0^d, |\alpha| = r\} \right) \\
&= (\text{span}\{1\} \oplus \mathcal{LP}^{r-1}) \oplus \text{span}\{\mathcal{L}\mathbf{x}^\alpha : \alpha \in \mathbb{N}_0^d, |\alpha| = r\} \\
&= \mathcal{P}_0^{r-1} \oplus \text{span}\{\mathcal{L}\mathbf{x}^\alpha : \alpha \in \mathbb{N}_0^d, |\alpha| = r\} \\
&= \mathcal{P}_0^{r-1} \oplus \text{span}\{\Delta_{\mathbf{x}}\mathbf{x}^\alpha + \nabla_{\mathbf{x}}\mathbf{x}^\alpha \cdot \nabla_{\mathbf{x}} \log p(\mathbf{x}) : \alpha \in \mathbb{N}_0^d, |\alpha| = r\} \\
&= \mathcal{P}_0^{r-1} \oplus \text{span}\left\{ \sum_{j=1}^d \alpha_j(\alpha_j - 1)x_j^{\alpha_j-2} \prod_{k \neq j} x_k^{\alpha_k} - \sum_{j=1}^d \alpha_j \mathbf{x}^\alpha : \alpha \in \mathbb{N}_0^d, |\alpha| = r \right\} \\
&= \mathcal{P}_0^{r-1} \oplus \mathcal{Q}^r.
\end{aligned}$$

To complete the inductive step we must therefore show that, for each $\alpha \in \mathbb{N}_0^d$ with $|\alpha| = r$, we have $\mathbf{x}^\alpha \in \text{span}\{1\} \oplus \mathcal{LP}^r$. Fix any $\alpha \in \mathbb{N}_0^d$ such that $|\alpha| = r$. Then

$$\phi(\mathbf{x}) = \sum_{j=1}^d \alpha_j(\alpha_j - 1)x_j^{\alpha_j-2} \prod_{k \neq j} x_k^{\alpha_k} - \sum_{j=1}^d \alpha_j \mathbf{x}^\alpha \in \mathcal{Q}^r.$$

and

$$\varphi(\mathbf{x}) = \frac{1}{\mathbf{1}^\top \alpha} \sum_{j=1}^d \alpha_j(\alpha_j - 1)x_j^{\alpha_j-2} \prod_{k \neq j} x_k^{\alpha_k} \in \mathcal{P}_0^{r-1}$$

because this polynomial is of order less than r . Since $\varphi - (\mathbf{1}^\top \alpha)^{-1} \phi \in \mathcal{P}_0^{r-1} \oplus \mathcal{Q}^r = \text{span}\{1\} \oplus \mathcal{LP}^r$ and

$$\varphi(\mathbf{x}) - \frac{1}{\mathbf{1}^\top \alpha} \phi(\mathbf{x}) = \frac{\sum_{j=1}^d \alpha_j}{\mathbf{1}^\top \alpha} \mathbf{x}^\alpha = \mathbf{x}^\alpha,$$

we conclude that $\mathbf{x}^\alpha \in \text{span}\{1\} \oplus \mathcal{LP}^r$. Thus we have shown that $\{\mathbf{x}^\alpha : \alpha \in \mathbb{N}_0^d, |\alpha| = r\} \subset \text{span}\{1\} \oplus \mathcal{LP}^r$ and this completes the argument. \square

F Proof of Lemma 4

Proof. The assumptions that the $\mathbf{x}^{(i)}$ are distinct and that k_0 is a positive-definite kernel imply that the matrix \mathbf{K}_0 is positive-definite and thus non-singular. Likewise, the assumption that the $\mathbf{x}^{(i)}$ are \mathcal{F} -unisolvant implies that the matrix \mathbf{P} has full rank. It follows that the block matrix in (12) is non-singular. The interpolation and semi-exactness conditions in Section 2.3 can be written in matrix form as

1. $K_0 \mathbf{a} + \mathbf{P} \mathbf{b} = \mathbf{f}$ (interpolation);
2. $\mathbf{P}^\top \mathbf{a} = \mathbf{0}$ (semi-exact).

The first of these is merely (10) in matrix form. To see how $\mathbf{P}^\top \mathbf{a} = \mathbf{0}$ is related to the semi-exactness requirement ($f_m = f$ whenever $f \in \mathcal{F}$), observe that for $f \in \mathcal{F}$ we have $\mathbf{f} = \mathbf{P} \mathbf{c}$ for some $\mathbf{c} \in \mathbb{R}^q$. Consequently, the interpolation condition should yield $\mathbf{b} = \mathbf{c}$ and $\mathbf{a} = \mathbf{0}$. The condition $\mathbf{P}^\top \mathbf{a} = \mathbf{0}$ enforces that $\mathbf{a} = \mathbf{0}$ in this case: multiplication of the interpolation equation with \mathbf{a}^\top yields $\mathbf{a}^\top K_0 \mathbf{a} + \mathbf{a}^\top \mathbf{P} \mathbf{b} = \mathbf{a}^\top \mathbf{P} \mathbf{c}$, which is then equivalent to $\mathbf{a}^\top K_0 \mathbf{a} = \mathbf{0}$. Because K_0 is positive-definite, the only possible $\mathbf{a} \in \mathbb{R}^m$ is $\mathbf{a} = \mathbf{0}$ and \mathbf{P} having full rank implies that $\mathbf{b} = \mathbf{c}$. Thus the coefficients \mathbf{a} and \mathbf{b} can be cast as the solution to the linear system

$$\begin{bmatrix} K_0 & \mathbf{P} \\ \mathbf{P}^\top & \mathbf{0} \end{bmatrix} \begin{bmatrix} \mathbf{a} \\ \mathbf{b} \end{bmatrix} = \begin{bmatrix} \mathbf{f} \\ \mathbf{0} \end{bmatrix}.$$

From (12) we get

$$\mathbf{b} = (\mathbf{P}^\top K_0^{-1} \mathbf{P})^{-1} \mathbf{P}^\top K_0^{-1} \mathbf{f},$$

where $\mathbf{P}^\top K_0^{-1} \mathbf{P}$ is non-singular because K_0 is non-singular and \mathbf{P} has full rank. Recognising that $b_1 = \mathbf{e}_1^\top \mathbf{b}$ for $\mathbf{e}_1 = (1, 0, \dots, 0) \in \mathbb{R}^q$ completes the argument. \square

G Nyström Approximation and Conjugate Gradient

In this appendix we describe how a Nyström approximation and the conjugate gradient method can be used to provide an approximation to the proposed method with reduced computational cost. To this end we consider a function of the form

$$\tilde{f}_{m_0}(\mathbf{x}) = \tilde{b}_1 + \sum_{i=1}^{q-1} \tilde{b}_{i+1} \mathcal{L} \phi_i(\mathbf{x}) + \sum_{i=1}^{m_0} \tilde{a}_i k_0(\mathbf{x}, \mathbf{x}^{(i)}), \quad (24)$$

where $m_0 \ll m$ represents a small subset of the m points in the dataset. Strategies for selection of a suitable subset are numerous (e.g., Alaoui and Mahoney, 2015; Rudi et al., 2015) but for simplicity in this work a uniform random subset was selected. Without loss of generality we denote this subset by the first m_0 indices in the dataset. The coefficients \mathbf{a} and \mathbf{b} in the proposed method (10) can be characterized as the solution to a kernel least-squares problem, the details of which are reserved for Appendix G.1. From this perspective it is natural to define the reduced coefficients $\tilde{\mathbf{a}}$ and $\tilde{\mathbf{b}}$ in (24) also as the solution to a kernel least-squares problem, the details of which are reserved for Appendix G.2. In taking this approach, the $(m+Q)$ -dimensional linear system in (12) becomes the (m_0+Q) -dimensional linear system

$$\begin{bmatrix} K_{0,m_0,m} K_{0,m,m_0} + \mathbf{P}_{m_0} \mathbf{P}_{m_0}^\top & K_{0,m_0,m} \mathbf{P} \\ \mathbf{P}^\top K_{0,m,m_0} & \mathbf{P}^\top \mathbf{P} \end{bmatrix} \begin{bmatrix} \tilde{\mathbf{a}} \\ \tilde{\mathbf{b}} \end{bmatrix} = \begin{bmatrix} K_{0,m_0,m} \mathbf{f} \\ \mathbf{P}^\top \mathbf{f} \end{bmatrix}. \quad (25)$$

Here $\mathbf{K}_{0,r,s}$ denotes the matrix formed by the first r rows and the first s columns of \mathbf{K}_0 . Similarly \mathbf{P}_r denotes the first r rows of \mathbf{P} . It can be verified that there is no approximation error when $m_0 = m$, with $\tilde{\mathbf{a}} = \mathbf{a}$ and $\tilde{\mathbf{b}} = \mathbf{b}$. This is a simple instance of a Nyström approximation and it can be viewed as a random projection method (Smola and Schölkopf, 2000; Williams and Seeger, 2001).

The computational complexity of computing this approximation to the proposed method is

$$O(mm_0^2 + mQ^2 + m_0^3 + Q^3),$$

which could still be quite high. For this reason, we now consider iterative, as opposed to direct, linear solvers for (25). In particular, we employ the conjugate gradient method to approximately solve this linear system. The performance of the conjugate gradient method is determined by the condition number of the linear system, and for this reason a preconditioner should be employed¹. In this work we considered the preconditioner

$$\begin{bmatrix} \mathbf{B}_1 & \mathbf{0} \\ \mathbf{0} & \mathbf{B}_2 \end{bmatrix}.$$

Following Rudi et al. (2017), \mathbf{B}_1 is the lower-triangular matrix resulting from a Cholesky decomposition

$$\mathbf{B}_1 \mathbf{B}_1^\top = \left(\frac{m}{m_0} \mathbf{K}_{0,m_0,m_0}^2 + \mathbf{P}_{m_0} \mathbf{P}_{m_0}^\top \right)^{-1},$$

the latter being an approximation to the inverse of $\mathbf{K}_{0,m_0,m} \mathbf{K}_{0,m,m_0} + \mathbf{P}_{m_0} \mathbf{P}_{m_0}^\top$ and obtained at $O(m_0^3 + Qm_0^2)$ cost. The matrix \mathbf{B}_2 is

$$\mathbf{B}_2 \mathbf{B}_2^\top = (\mathbf{P}^\top \mathbf{P})^{-1},$$

which uses the pre-computed matrix $\mathbf{P}^\top \mathbf{P}$ and is of $O(Q^3)$ complexity. Thus we obtain a preconditioned linear system

$$\begin{bmatrix} \mathbf{B}_1^\top (\mathbf{K}_{0,m_0,m} \mathbf{K}_{0,m,m_0} + \mathbf{P}_{m_0} \mathbf{P}_{m_0}^\top) \mathbf{B}_1 & \mathbf{B}_1^\top \mathbf{K}_{0,m_0,m} \mathbf{P} \mathbf{B}_2 \\ \mathbf{B}_2^\top \mathbf{P}^\top \mathbf{K}_{0,m,m_0} \mathbf{B}_1 & \mathbf{I} \end{bmatrix} \begin{bmatrix} \tilde{\mathbf{a}} \\ \tilde{\mathbf{b}} \end{bmatrix} = \begin{bmatrix} \mathbf{B}_1^\top \mathbf{K}_{0,m_0,m} \mathbf{f} \\ \mathbf{B}_2^\top \mathbf{P}^\top \mathbf{f} \end{bmatrix}.$$

The coefficients $\tilde{\mathbf{a}}$ and $\tilde{\mathbf{b}}$ of \tilde{f}_{m_0} are related to the solution $(\tilde{\mathbf{a}}, \tilde{\mathbf{b}})$ of this preconditioner linear system via $\tilde{\mathbf{a}} = \mathbf{B}_1^{-1} \tilde{\mathbf{a}}$ and $\tilde{\mathbf{b}} = \mathbf{B}_2^{-1} \tilde{\mathbf{b}}$, which is an upper-triangular linear system solved at quadratic cost.

The above procedure leads to a more computationally (time and space) efficient procedure, and we denote the resulting estimator as $I_{\text{ASECF}}(f) = \tilde{b}_1$. Further extensions could be considered; for example non-uniform sampling for the random projection via leverage scores (Rudi et al., 2015).

For the examples in Section 3, we consider $m_0 = \lceil \sqrt{m} \rceil$ where $\lceil \cdot \rceil$ denotes the ceiling function. We use the R package `Rlinsolve` to perform conjugate gradient,

¹A linear system $\mathbf{A}\mathbf{x} = \mathbf{b}$ can be *preconditioned* by an invertible matrix \mathbf{P} to produce $\mathbf{P}^\top \mathbf{A} \mathbf{P} \mathbf{z} = \mathbf{P}^\top \mathbf{b}$. The solution \mathbf{z} is related to \mathbf{x} via $\mathbf{x} = \mathbf{P}\mathbf{z}$.

where we specify the tolerance to be 10^{-5} . The initial value for the conjugate gradient procedure was the choice of $\tilde{\mathbf{a}}$ and $\tilde{\mathbf{b}}$ that leads to the Monte Carlo estimate, $\tilde{\mathbf{a}} = \mathbf{0}$ and $\tilde{\mathbf{b}} = \mathbf{B}_2^{-1} \mathbf{e}_1 \frac{1}{m} \sum_{i=1}^m f(\mathbf{x}^{(i)})$. In our examples, we did not see a computational speed up from the use of conjugate gradient, likely due to the relatively small values of m involved.

G.1 Kernel Least-Squares Characterization

Here we explain how the interpolant f_m in (10) can be characterized as the solution to the constrained kernel least-squares problem

$$\arg \min_{\mathbf{a}, \mathbf{b}} \frac{1}{m} \sum_{i=1}^m [f(\mathbf{x}^{(i)}) - f_m(\mathbf{x}^{(i)})]^2 \quad \text{s.t.} \quad f_m = f \quad \text{for all} \quad f \in \mathcal{F}.$$

To see this, note that similar reasoning to that in Appendix F allows us to formulate the problem using matrices as

$$\arg \min_{\mathbf{a}, \mathbf{b}} \|\mathbf{f} - \mathbf{K}_0 \mathbf{a} - \mathbf{P} \mathbf{b}\|^2 \quad \text{s.t.} \quad \mathbf{P}^\top \mathbf{a} = \mathbf{0}. \quad (26)$$

This is a quadratic minimization problem subject to the constraint $\mathbf{P}^\top \mathbf{a} = \mathbf{0}$ and therefore the solution is given by the Karush–Kuhn–Tucker matrix equation

$$\begin{bmatrix} \mathbf{K}_0^2 & \mathbf{K}_0 \mathbf{P} & \mathbf{P} \\ \mathbf{P}^\top \mathbf{K}_0 & \mathbf{P}^\top \mathbf{P} & \mathbf{0} \\ \mathbf{P}^\top & \mathbf{0} & \mathbf{0} \end{bmatrix} \begin{bmatrix} \mathbf{a} \\ \mathbf{b} \\ \mathbf{c} \end{bmatrix} = \begin{bmatrix} \mathbf{K} \mathbf{f} \\ \mathbf{P}^\top \mathbf{f} \\ \mathbf{0} \end{bmatrix}. \quad (27)$$

Now, we are free to add a multiple, \mathbf{P} , of the third row to the first row, which produces

$$\begin{bmatrix} \mathbf{K}_0^2 + \mathbf{P} \mathbf{P}^\top & \mathbf{K}_0 \mathbf{P} & \mathbf{P} \\ \mathbf{P}^\top \mathbf{K}_0 & \mathbf{P}^\top \mathbf{P} & \mathbf{0} \\ \mathbf{P}^\top & \mathbf{0} & \mathbf{0} \end{bmatrix} \begin{bmatrix} \mathbf{a} \\ \mathbf{b} \\ \mathbf{c} \end{bmatrix} = \begin{bmatrix} \mathbf{K} \mathbf{f} \\ \mathbf{P}^\top \mathbf{f} \\ \mathbf{0} \end{bmatrix}.$$

Next, we make the *ansatz* that $\mathbf{c} = \mathbf{0}$ and seek a solution to the reduced linear system

$$\begin{bmatrix} \mathbf{K}_0^2 + \mathbf{P} \mathbf{P}^\top & \mathbf{K}_0 \mathbf{P} \\ \mathbf{P}^\top \mathbf{K}_0 & \mathbf{P}^\top \mathbf{P} \end{bmatrix} \begin{bmatrix} \mathbf{a} \\ \mathbf{b} \end{bmatrix} = \begin{bmatrix} \mathbf{K} \mathbf{f} \\ \mathbf{P}^\top \mathbf{f} \end{bmatrix}.$$

This is the same as

$$\begin{bmatrix} \mathbf{K}_0 & \mathbf{P} \\ \mathbf{P}^\top & \mathbf{0} \end{bmatrix} \begin{bmatrix} \mathbf{K}_0 & \mathbf{P} \\ \mathbf{P}^\top & \mathbf{0} \end{bmatrix} = \begin{bmatrix} \mathbf{K}_0 & \mathbf{P} \\ \mathbf{P}^\top & \mathbf{0} \end{bmatrix} \begin{bmatrix} \mathbf{f} \\ \mathbf{0} \end{bmatrix}$$

and thus, if the block matrix can be inverted, we have

$$\begin{bmatrix} \mathbf{K}_0 & \mathbf{P} \\ \mathbf{P}^\top & \mathbf{0} \end{bmatrix} = \begin{bmatrix} \mathbf{f} \\ \mathbf{0} \end{bmatrix} \quad (28)$$

as claimed. Existence of a solution to (28) establishes a solution to the original system (27) and justifies the *ansatz*. Moreover, the fact that a solution to (28) exists was established in Lemma 4.

G.2 Nyström Approximation

To develop a Nyström approximation, our starting point is the kernel least-squares characterization of the proposed estimator in (26). In particular, the same least-squares problem can be considered for the Nyström approximation in (24):

$$\arg \min_{\tilde{\mathbf{a}}, \tilde{\mathbf{b}}} \|\mathbf{f} - \mathbf{K}_{0,m,m_0} \tilde{\mathbf{a}} - \tilde{\mathbf{P}} \tilde{\mathbf{b}}\|_2^2 \quad \text{s.t.} \quad \mathbf{P}_{m_0}^\top \tilde{\mathbf{a}} = \mathbf{0}.$$

This least-squares problem can be formulated as

$$\begin{aligned} & \arg \min_{\tilde{\mathbf{a}}, \tilde{\mathbf{b}}} (\mathbf{f} - \mathbf{K}_{0,m,m_0} \tilde{\mathbf{a}} - \tilde{\mathbf{P}} \tilde{\mathbf{b}})^\top (\mathbf{f} - \mathbf{K}_{0,m,m_0} \tilde{\mathbf{a}} - \tilde{\mathbf{P}} \tilde{\mathbf{b}}) \\ &= \arg \min_{\tilde{\mathbf{a}}, \tilde{\mathbf{b}}} \left[\mathbf{f}^\top \mathbf{f} - \mathbf{f}^\top \mathbf{K}_{0,m,m_0} \tilde{\mathbf{a}} - \mathbf{f}^\top \tilde{\mathbf{P}} \tilde{\mathbf{b}} - \tilde{\mathbf{a}}^\top \mathbf{K}_{0,m,m_0} \mathbf{f} + \tilde{\mathbf{a}}^\top \mathbf{K}_{0,m_0,m} \mathbf{K}_{0,m,m_0} \tilde{\mathbf{a}} \right. \\ & \quad \left. + \tilde{\mathbf{a}}^\top \mathbf{K}_{0,m_0,m} \tilde{\mathbf{P}} \tilde{\mathbf{b}} - \tilde{\mathbf{b}}^\top \mathbf{P}^\top \mathbf{f} - \tilde{\mathbf{b}}^\top \mathbf{P}^\top \mathbf{K}_{0,m,m_0} \tilde{\mathbf{a}} - \tilde{\mathbf{b}}^\top \mathbf{P}^\top \tilde{\mathbf{P}} \tilde{\mathbf{b}} \right] \\ &= \arg \min_{\tilde{\mathbf{a}}, \tilde{\mathbf{b}}} \begin{bmatrix} \tilde{\mathbf{a}} \\ \tilde{\mathbf{b}} \end{bmatrix}^\top \begin{bmatrix} \mathbf{K}_{0,m_0,m} \mathbf{K}_{0,m,m_0} & \mathbf{K}_{0,m_0,m} \mathbf{P} \\ \mathbf{P}^\top \mathbf{K}_{0,m,m_0} & \mathbf{P}^\top \mathbf{P} \end{bmatrix} \begin{bmatrix} \tilde{\mathbf{a}} \\ \tilde{\mathbf{b}} \end{bmatrix} - 2 \begin{bmatrix} \mathbf{K}_{0,m_0,m} \mathbf{f} \\ \mathbf{P}^\top \mathbf{f} \end{bmatrix} \begin{bmatrix} \tilde{\mathbf{a}} \\ \tilde{\mathbf{b}} \end{bmatrix} + \mathbf{f}^\top \mathbf{f} \end{aligned}$$

This is a quadratic minimization problem subject to the constraint $\mathbf{P}_{m_0}^\top \tilde{\mathbf{a}} = \mathbf{0}$ and so the solution is given by the Karush–Kuhn–Tucker matrix equation

$$\begin{bmatrix} \mathbf{K}_{0,m_0,m} \mathbf{K}_{0,m,m_0} & \mathbf{K}_{0,m_0,m} \mathbf{P} & \mathbf{P}_{m_0} \\ \mathbf{P}^\top \mathbf{K}_{0,m,m_0} & \mathbf{P}^\top \mathbf{P} & \mathbf{0} \\ \mathbf{P}_{m_0}^\top & \mathbf{0} & \mathbf{0} \end{bmatrix} \begin{bmatrix} \tilde{\mathbf{a}} \\ \tilde{\mathbf{b}} \\ \tilde{\mathbf{c}} \end{bmatrix} = \begin{bmatrix} \mathbf{K}_{0,m_0,m} \mathbf{f} \\ \mathbf{P}^\top \mathbf{f} \\ \mathbf{0} \end{bmatrix}. \quad (29)$$

Following an identical argument to that in Appendix G.1, we first add \mathbf{P}_{m_0} times the third row to the first row to obtain

$$\begin{bmatrix} \mathbf{K}_{0,m_0,m} \mathbf{K}_{0,m,m_0} + \mathbf{P}_{m_0} \mathbf{P}_{m_0}^\top & \mathbf{K}_{0,m_0,m} \mathbf{P} & \mathbf{P}_{m_0} \\ \mathbf{P}^\top \mathbf{K}_{0,m,m_0} & \mathbf{P}^\top \mathbf{P} & \mathbf{0} \\ \mathbf{P}_{m_0}^\top & \mathbf{0} & \mathbf{0} \end{bmatrix} \begin{bmatrix} \tilde{\mathbf{a}} \\ \tilde{\mathbf{b}} \\ \tilde{\mathbf{c}} \end{bmatrix} = \begin{bmatrix} \mathbf{K}_{0,m_0,m} \mathbf{f} \\ \mathbf{P}^\top \mathbf{f} \\ \mathbf{0} \end{bmatrix}.$$

Taking again the *ansatz* that $\tilde{\mathbf{c}} = \mathbf{0}$ requires us to solve the reduced linear system

$$\begin{bmatrix} \mathbf{K}_{0,m_0,m} \mathbf{K}_{0,m,m_0} + \mathbf{P}_{m_0} \mathbf{P}_{m_0}^\top & \mathbf{K}_{0,m_0,m} \mathbf{P} \\ \mathbf{P}^\top \mathbf{K}_{0,m,m_0} & \mathbf{P}^\top \mathbf{P} \end{bmatrix} \begin{bmatrix} \tilde{\mathbf{a}} \\ \tilde{\mathbf{b}} \end{bmatrix} = \begin{bmatrix} \mathbf{K}_{0,m_0,m} \mathbf{f} \\ \mathbf{P}^\top \mathbf{f} \end{bmatrix}. \quad (30)$$

As in Appendix G.1, the existence of a solution to (30) implies a solution to (29) and justifies the *ansatz*.

H The Effect of the Kernel and Tuning Approach

In this appendix we investigate the sensitivity of kernel-based methods (I_{CF} , I_{SECF} and I_{ASECF}) to the kernel and its parameter using the Gaussian example of Section 3.1. Specifically we compare the three kernels described in Appendix B, the

Gaussian, Matérn and rational quadratic kernels, when the parameter, λ , is chosen using either cross-validation or the median heuristic (Garreau et al., 2017). For the Matérn kernel, we fix the smoothness parameter at $\nu = 4.5$.

In the cross-validation approach,

$$\lambda_{\text{CV}} \in \arg \min \sum_{i=1}^5 \sum_{j=1}^{m_5} [f(\mathbf{x}^{(i,j)}) - f_{i,\lambda}(\mathbf{x}^{(i,j)})]^2, \quad (31)$$

where $m_5 = \lfloor m/5 \rfloor$, $f_{i,\lambda}$ denotes an interpolant of the form (10) to f at the points $\{\mathbf{x}^{(i,j)} : j = 1, \dots, m_5\}$ with kernel parameter λ , and $\mathbf{x}^{(i,j)}$ is the j th point in the i th fold. In general (31) is an intractable optimization problem and we therefore perform a grid-based search. Here we consider $\lambda \in 10^{\{-1.5, -1, -0.5, 0, 0.5, 1\}}$.

The median heuristic described in Garreau et al. (2017) is the choice of the bandwidth

$$\tilde{\lambda} = \sqrt{\frac{1}{2} \text{Med} \left\{ \|\mathbf{x}^{(i)} - \mathbf{x}^{(j)}\|^2 : 1 \leq i < j \leq m \right\}}$$

for functions of the form $k(\mathbf{x}, \mathbf{y}) = \varphi(\|\mathbf{x} - \mathbf{y}\|/\lambda)$, where Med is the empirical median. This heuristic can be used for the Gaussian, Matérn and rational quadratic kernels, which all fit into this framework.

Figures 6 and 7 show the statistical efficiency of each combination of kernel and tuning approach for $m = 1000$ and $d = 4$, respectively. The outcome that the performance of I_{SECF} and I_{ASECF} are less sensitive to the kernel choice than I_{CF} is intuitive when considering the fact that semi-exact control functionals enforce exactness on $f \in \mathcal{F}$.

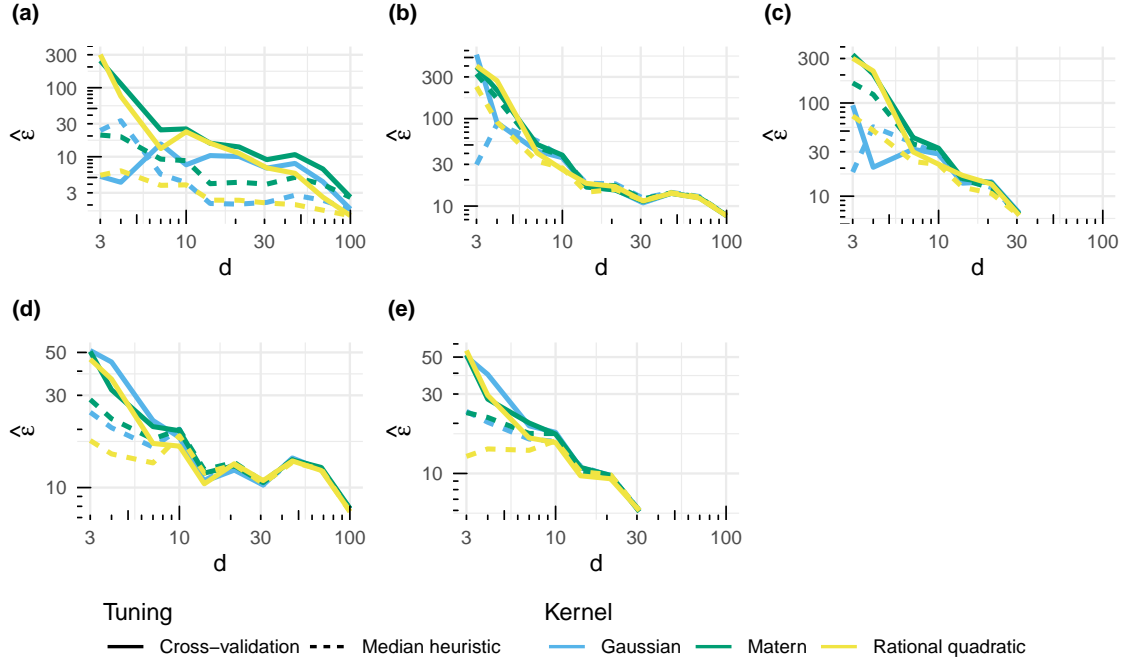


Figure 6: Gaussian example, estimated statistical efficiency for $N = 1000$ using different kernels and tuning approaches. The estimators are (a) I_{CF} , (b) I_{SECF} with polynomial order $r = 1$, (c) I_{SECF} with $r = 2$, (d) I_{ASECF} with $r = 1$ and (e) I_{ASECF} with $r = 2$.

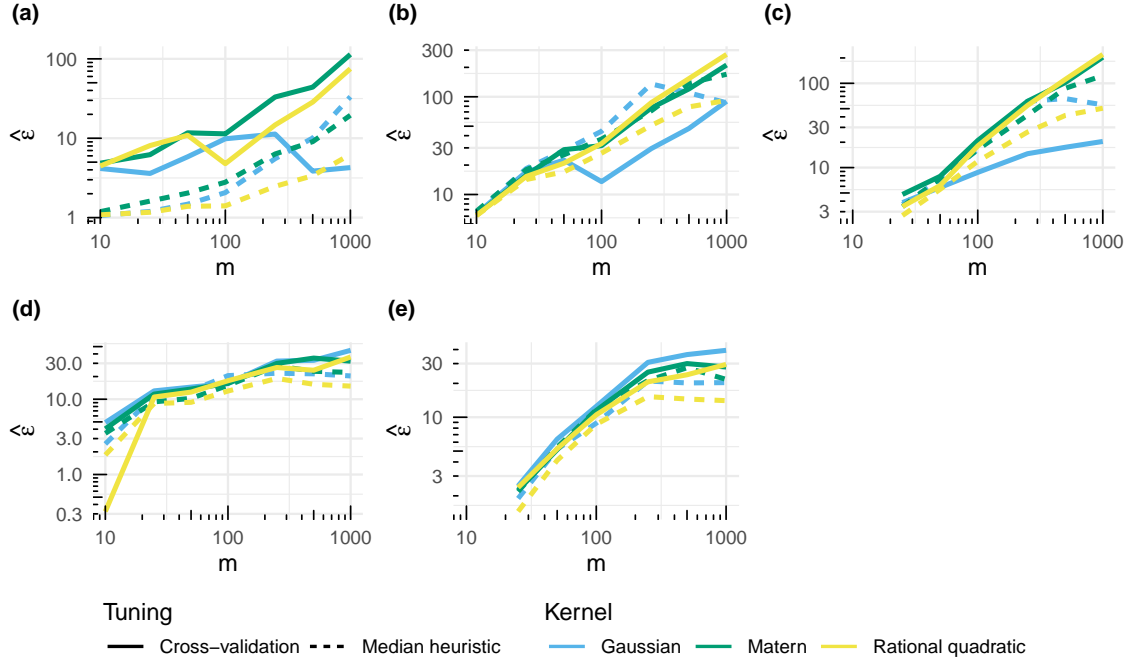


Figure 7: Gaussian example, estimated statistical efficiency for $d = 4$ using different kernels and tuning approaches. The estimators are (a) I_{CF} , (b) I_{SECF} with polynomial order $r = 1$, (c) I_{SECF} with $r = 2$, (d) I_{ASECF} with $r = 1$ and (e) I_{ASECF} with $r = 2$.

I Empirical Results for the Unadjusted Langevin Algorithm

Recall that the proposed method does not require that the $\mathbf{x}^{(i)}$ form an empirical approximation to p . It is therefore interesting to investigate the behaviour of the method when the $(\mathbf{x}^{(i)})_{i=1}^{\infty}$ arise as a Markov chain that does not leave p invariant. Figures 8 and 9 show results when the unadjusted Langevin algorithm is used rather than the Metropolis-adjusted Langevin algorithm which is behind Figures 3 and 4 of the main text. The benefit of the proposed method for samplers that do not leave p invariant is evident through its reduced bias compared to I_{ZV} and I_{MC} in Figure 10. Recall that the unadjusted Langevin algorithm (Parisi, 1981; Ermak, 1975) is defined by

$$\mathbf{x}^{(i+1)} = \mathbf{x}^{(i)} + \frac{h^2}{2} \Sigma \nabla_{\mathbf{x}} \log P_{\mathbf{x}|\mathbf{y}}(\mathbf{x}^{(i)} | \mathbf{y}) + \epsilon_{i+1},$$

for $i = 1, \dots, m - 1$ where $\mathbf{x}^{(1)}$ is a fixed point with high posterior support and $\epsilon_{i+1} \sim \mathcal{N}(\mathbf{0}, h^2 \Sigma)$. Step sizes of $h = 0.9$ for the sonar example and $h = 1.1$ for the capture-recapture example were selected.

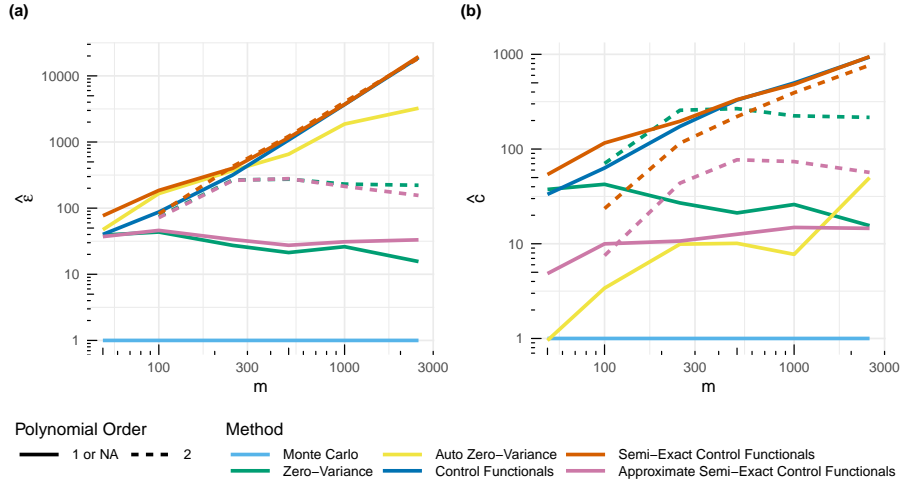


Figure 8: Recapture example (a) estimated *statistical efficiency* and (b) estimated *computational efficiency* when the unadjusted Langevin algorithm is used in place of the Metropolis-adjusted Langevin algorithm. Efficiency here is reported as an average over the 11 expectations of interest.

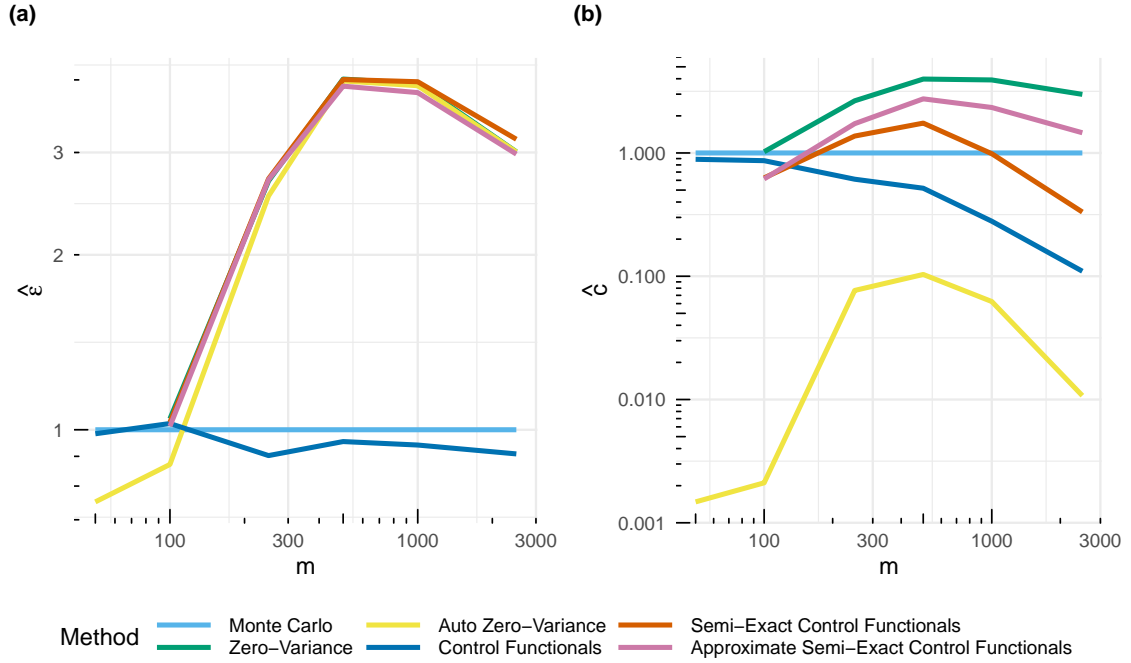


Figure 9: Sonar example (a) estimated *statistical efficiency* and (b) estimated *computational efficiency* when the unadjusted Langevin algorithm is used in place of the Metropolis-adjusted Langevin algorithm.

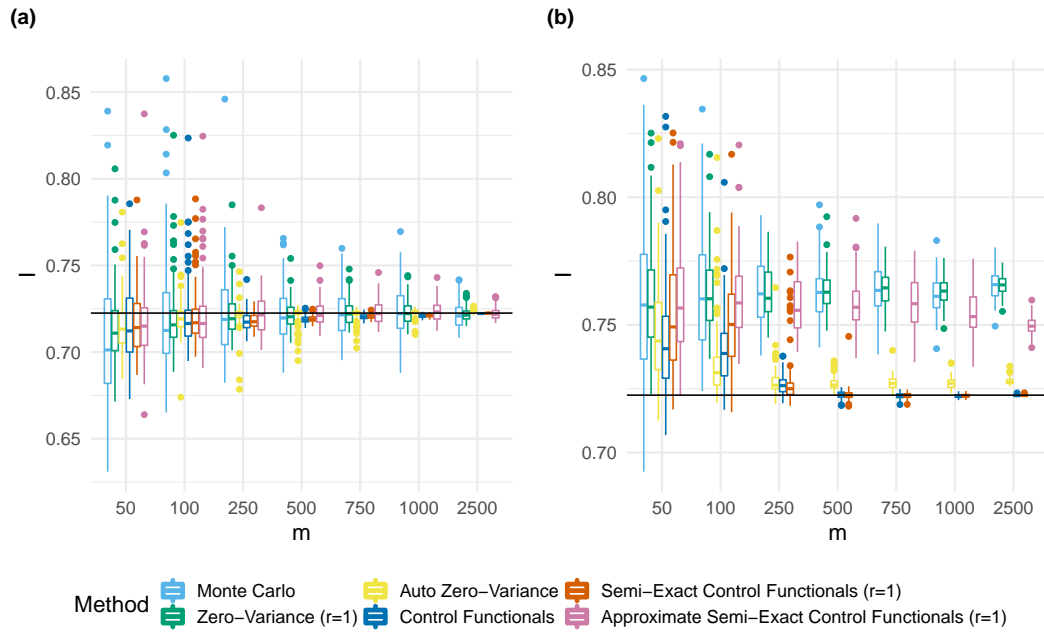


Figure 10: Recapture example (a) boxplots of 100 estimates of $\int x_1 P_{\mathbf{x}|\mathbf{y}} d\mathbf{x}$ when the Metropolis-adjusted Langevin algorithm is used for sampling and (b) boxplots of 100 estimates of $\int x_1 P_{\mathbf{x}|\mathbf{y}} d\mathbf{x}$ when the unadjusted Langevin algorithm is used for sampling. The black horizontal line represents the gold standard of approximation.

J Proof of Proposition 1

Proof. For any weights $\mathbf{v} = (v_1, \dots, v_m) \in \mathbb{R}^m$ and $g \in \mathcal{G}(k_0)$ there is a standard worst-case error decomposition (e.g., Dick et al., 2013, Section 3)

$$\left| \int g(\mathbf{x})p(\mathbf{x}) \, d\mathbf{x} - \sum_{i=1}^m v_i g(\mathbf{x}^{(i)}) \right| \leq \|g\|_{\mathcal{G}(k_0)} e(\mathbf{v}) \quad (32)$$

where

$$e(\mathbf{v}) = \sup_{\|g\|_{\mathcal{G}(k_0)} \leq 1} \left| \int g(\mathbf{x})p(\mathbf{x}) \, d\mathbf{x} - \sum_{i=1}^m v_i g(\mathbf{x}^{(i)}) \right|$$

is the worst-case integration error in $\mathcal{G}(k_0)$. Due to the reproducing kernel Hilbert space structure of $\mathcal{G}(k_0)$ the worst-case error has the explicit form (Oettershagen, 2017, Corollary 3.6)

$$e(\mathbf{v}) = \left(\int \int k_0(\mathbf{x}, \mathbf{y}) p(\mathbf{x}) p(\mathbf{y}) \, d\mathbf{x} \, d\mathbf{y} - 2 \sum_{i=1}^m v_i \int k_0(\mathbf{x}, \mathbf{x}^{(i)}) p(\mathbf{x}) \, d\mathbf{x} + \mathbf{v}^\top \mathbf{K}_0 \mathbf{v} \right)^{1/2}. \quad (33)$$

From (9) it follows that the first two terms in (33) vanish

$$e(\mathbf{v}) = (\mathbf{v}^\top \mathbf{K}_0 \mathbf{v})^{1/2}. \quad (34)$$

Let $f_m(\cdot; f)$ denote the interpolant (10), making the (linear) dependence on f explicit. The interpolant is a linear operator and the semi-exactness property means that $f_m(\cdot; h) = h$ for all $h \in \mathcal{F}$. Thus if $f = h + g$ with $h \in \mathcal{F}$ and $g \in \mathcal{G}(k_0)$, then it follows from (32) and (34) that

$$\begin{aligned} |I(f) - I_{\text{SECF}}(f)| &= |I(f) - I(f_m(\cdot; f))| \\ &= |I(h + g) - I(f_m(\cdot; h + g))| \\ &= |I(h + g) - I(h + f_m(\cdot; g))| \\ &= |I(h) + I(g) - I(h) - I(f_m(\cdot; g))| \\ &= |I(g) - I(f_m[g])| \\ &\leq \|g\|_{\mathcal{G}(k_0)} e(\mathbf{w}) \\ &= \|g\|_{\mathcal{G}(k_0)} (\mathbf{w}^\top \mathbf{K}_0 \mathbf{w})^{1/2}. \end{aligned}$$

Since this argument holds for any decomposition $f = h + g$ with $h \in \mathcal{F}$ and $g \in \mathcal{G}(k_0)$ we have that

$$|I(f) - I_{\text{SECF}}(f)| \leq \inf_{\substack{f=h+g \\ h \in \mathcal{F}, g \in \mathcal{G}(k_0)}} \|g\|_{\mathcal{G}(k_0)} (\mathbf{w}^\top \mathbf{K}_0 \mathbf{w})^{1/2} = |f|_{k_0, \mathcal{F}} (\mathbf{w}^\top \mathbf{K}_0 \mathbf{w})^{1/2}$$

as claimed. Finally, that the \mathbf{w} have minimal worst-case error among all weights that integrate functions in \mathcal{F} exactly is a consequence of Theorem 2.7, where the weights w_k are our \mathbf{w} in (14), and Remark D.1 in Karvonen et al. (2018). \square

K Proof of Theorem 1

Proof. From Assumption A2 and Lemma 4 we have that $(\mathbf{P}^\top \mathbf{K}_0^{-1} \mathbf{P})^{-1}$ is almost surely well-defined. From Assumption A4 and Proposition 1 we have that

$$(I(f) - I_{\text{SECF}}(f))^2 \leq |f|_{k_0, \mathcal{F}}^2 \mathbf{w}^\top \mathbf{K}_0 \mathbf{w}$$

and plugging in the expression for \mathbf{w} in (14), we have that

$$(I(f) - I_{\text{SECF}}(f))^2 \leq |f|_{k_0, \mathcal{F}}^2 [(\mathbf{P}^\top \mathbf{K}_0^{-1} \mathbf{P})^{-1}]_{11}.$$

It therefore suffices to show that $[(\mathbf{P}^\top \mathbf{K}_0^{-1} \mathbf{P})^{-1}]_{11} \rightarrow 0$ in probability as $m \rightarrow \infty$. To this end, let $[\Psi]_{i,j} := \mathcal{L}\phi_j(\mathbf{x}^{(i)})$ and consider the block matrix

$$\frac{\mathbf{P}^\top \mathbf{K}_0^{-1} \mathbf{P}}{\mathbf{1}^\top \mathbf{K}_0^{-1} \mathbf{1}} = \begin{bmatrix} 1 & \frac{\mathbf{1}^\top \mathbf{K}_0^{-1} \Psi}{\mathbf{1}^\top \mathbf{K}_0^{-1} \mathbf{1}} \\ \frac{\Psi^\top \mathbf{K}_0^{-1} \mathbf{1}}{\mathbf{1}^\top \mathbf{K}_0^{-1} \mathbf{1}} & \frac{\Psi^\top \mathbf{K}_0^{-1} \Psi}{\mathbf{1}^\top \mathbf{K}_0^{-1} \mathbf{1}} \end{bmatrix} \quad (35)$$

From the block matrix inversion formula we have that

$$\begin{aligned} \left[\left(\frac{\mathbf{P}^\top \mathbf{K}_0^{-1} \mathbf{P}}{\mathbf{1}^\top \mathbf{K}_0^{-1} \mathbf{1}} \right)^{-1} \right]_{1,1} &= \left[1 - \frac{\mathbf{1}^\top \mathbf{K}_0^{-1} \Psi (\Psi^\top \mathbf{K}_0^{-1} \Psi)^{-1} \Psi^\top \mathbf{K}_0^{-1} \mathbf{1}}{\mathbf{1}^\top \mathbf{K}_0^{-1} \mathbf{1}} \right]^{-1} \\ &= \left[1 - \frac{\langle \mathbf{1}, \Pi \mathbf{1} \rangle_{\mathbf{K}_0^{-1}}}{\langle \mathbf{1}, \mathbf{1} \rangle_{\mathbf{K}_0^{-1}}} \right]^{-1}. \end{aligned} \quad (36)$$

Since $\Pi = \Psi(\Psi^\top \mathbf{K}_0^{-1} \Psi)^{-1} \Psi^\top \mathbf{K}_0^{-1}$ and

$$\begin{aligned} \|\Pi \mathbf{1}\|_{\mathbf{K}_0^{-1}}^2 &= \mathbf{1}^\top \Pi^\top \mathbf{K}_0^{-1} \Pi \mathbf{1} \\ &= \mathbf{1}^\top \mathbf{K}_0^{-1} \Psi (\Psi^\top \mathbf{K}_0^{-1} \Psi)^{-1} \Psi^\top \mathbf{K}_0^{-1} \Psi (\Psi^\top \mathbf{K}_0^{-1} \Psi)^{-1} \Psi^\top \mathbf{K}_0^{-1} \mathbf{1} \\ &= \mathbf{1}^\top \mathbf{K}_0^{-1} \Psi (\Psi^\top \mathbf{K}_0^{-1} \Psi)^{-1} \Psi^\top \mathbf{K}_0^{-1} \mathbf{1} \\ &= \mathbf{1}^\top \mathbf{K}_0^{-1} \Pi \mathbf{1} \\ &= \langle \mathbf{1}, \Pi \mathbf{1} \rangle_{\mathbf{K}_0^{-1}}, \end{aligned}$$

our Assumption A3 implies that (36) is almost surely asymptotically bounded, say by a constant $C \in [0, \infty)$. In other words, it almost surely holds that

$$[(\mathbf{P}^\top \mathbf{K}_0^{-1} \mathbf{P})^{-1}]_{11} \leq C(\mathbf{1}^\top \mathbf{K}_0^{-1} \mathbf{1})^{-1}$$

for all sufficiently large m . The term $(\mathbf{1}^\top \mathbf{K}_0^{-1} \mathbf{1})^{-1}$ on the right hand side is recognised as the (squared) kernel Stein discrepancy (Chwialkowski et al., 2016; Liu et al., 2016) of the empirical measure $\sum_{i=1}^m w_i \delta(\mathbf{x}^{(i)})$ where the weights $\mathbf{w} = [w_1, \dots, w_m]^\top$ minimise this discrepancy subject to $\mathbf{1}^\top \mathbf{w} = 1$. Let $\tilde{\mathbf{w}}$ denote weights that minimise this discrepancy subject to $\mathbf{1}^\top \tilde{\mathbf{w}} = 1$ and $\tilde{\mathbf{w}} \geq \mathbf{0}$. From Assumption A1 and Theorem 1 of Hodgkinson et al. (2020), we have that the kernel Stein discrepancy of the empirical measure $\sum_{i=1}^m \tilde{w}_i \delta(\mathbf{x}^{(i)})$ converges to zero in probability as $m \rightarrow \infty$. Since the discrepancy associated to the weights \mathbf{w} is no greater than that associated to the weights $\tilde{\mathbf{w}}$, it follows that $(\mathbf{1}^\top \mathbf{K}_0^{-1} \mathbf{1})^{-1} \rightarrow 0$ in probability as $m \rightarrow \infty$, as required. \square